

**ELECTRIC FIELD ALIGNMENT OF CELLULOSE BASED-POLYMER
NANOCOMPOSITES**

A Dissertation

by

SANJAY VARMA KALIDINDI

Submitted to the Office of Graduate Studies of
Texas A&M University
in partial fulfillment of the requirements for the degree of

DOCTOR OF PHILOSOPHY

May 2012

Major Subject: Materials Science and Engineering

Electric Field Alignment of Cellulose Based-Polymer Nanocomposites

Copyright 2012 Sanjay Varma Kalidindi

**ELECTRIC FIELD ALIGNMENT OF CELLULOSE BASED-POLYMER
NANOCOMPOSITES**

A Dissertation

by

SANJAY VARMA KALIDINDI

Submitted to the Office of Graduate Studies of
Texas A&M University
in partial fulfillment of the requirements for the degree of

DOCTOR OF PHILOSOPHY

Approved by:

Chair of Committee,	Zoubeida Ounaies
Committee Members,	Hung-Jue Sue
	Ramesh Talreja
	Choongho Yu
Intercollegiate Faculty Chair,	Ibrahim Karaman

May 2012

Major Subject: Materials Science and Engineering

ABSTRACT

Electric Field Alignment of Cellulose Based-Polymer Nanocomposites.

(May 2012)

Sanjay Varma Kalidindi, B.E., Vellore Engineering College;

M.S., University of Texas – Pan American

Chair of Advisory Committee: Dr. Zoubeida Ounaies

Cellulose whiskers (CWs) obtained from naturally occurring cellulose are nano-inclusions which show a lot of promise as mechanical reinforcements in polymers. Typically, a relatively high content is added to realize improvement in effective mechanical behavior. This enhancement in modulus is usually followed by a modest increase in strength but generally the ductility and toughness decrease. Our approach is to use small concentrations of CWs so as not to detrimentally affect processability, toughness and ductility. By aligning the small concentrations, we target the same kind of improvement in modulus and strength as reported in the literature, but at much smaller volume contents.

In this work, we investigate the effect of AC electric field on the alignment of dispersed nanoscale CW in a polymer. Polyvinyl acetate (PVAc) is used as the model polymer because of the good interaction between CWs and PVAc. A low concentration of 0.4wt% was used for the study. Two dispersion methods, namely basic and modified, were developed. The basic method led to micron scale dispersion. Using the modified

method, CWs were individually dispersed in PVAc with average lengths and diameters of 260 nm and 8 nm respectively yielding an aspect ratio of approximately 30. The behavior of CWs (alignment and chain formation) under an applied electric field was found to be a function of applied electric field magnitude, frequency and duration. Following alignment, the CW/PVAc nanocomposites are thermally dried in the presence of electric field to maintain the aligned microstructure. Improvements in dielectric constant and mechanical properties were observed for the aligned cases as compared to random case and pure PVAc. The optimal electric field magnitude, frequency and duration for the alignment and chain formation were found to be $200V_{pp}/mm$, 50 KHz for duration of 20 minutes for the microcomposite and $250V_{pp}/mm$, 10KHz for a duration of 1hr for the nanocomposite. At 0.4wt% concentration, 21% increase in dielectric constant for the optimal nanocomposite case. Above T_g , a 680% improvement in elastic modulus at 0.4wt % concentration for the optimal nanocomposite case. The reason for the significant reinforcement is attributed to alignment (rotation and chain formation) and chain-chain interaction (3D network formation and hydrogen bonding).

DEDICATION

This dissertation is dedicated to my family.

ACKNOWLEDGEMENTS

First and foremost, I would like to thank my advisor and mentor, Dr. Zoubeida Ounaies for her guidance and support throughout my research and graduate study at Texas A&M University. Working with her has been a wonderful and rewarding experience. Her words of encouragement and patience have helped me immensely. I will always be grateful to her. I would like to thank, Dr. Hung-Jue Sue, Dr. Ramesh Talreja and Dr. Choongho Yu for serving on my committee. Their guidance and support throughout the course of this research is greatly appreciated.

I would like to thank our collaborator, Dr. Hamid Kaddami and his research group at University of Cadi-Ayyad, Morocco for providing the material, valuable insight and expertise to help me with my research.

Thanks also go to my friends and colleagues and the department faculty and staff of Aerospace Engineering and Material Science and Engineering for making my time at Texas A&M University a great experience.

I would like to thank my colleagues at Electroactive Materials Characterization Laboratory, especially Sumanth Banda, Sujay Deshmukh, Amira Brahoumi, Hassene Ben Atitallah, Payam Khodaparast and Nirmal Shankar for their help and support.

Finally, I would like to thank my parents, brother, grandparents and extended family for their never ending love, encouragement, and support. Special thanks to my uncle B. V. K Raju who encouraged me to pursue my graduate studies. Without their support and encouragement, I wouldn't have made it this far.

NOMENCLATURE

CWs	Cellulose whiskers
MFCs	Microfibrillated cellulose
DMA	Dynamic mechanical analysis
AFM	Atomic force microscopy
PVAc	Polyvinyl Acetate
DMF	Dimethyl Formamide
OM	Optical microscopy
SEM	Scanning electron microscopy
DSC	Differential scanning calorimetry
TGA	Thermogravimetric analysis
T_g	Glass transition temperature
E'	Storage modulus
SF	Unidirectional short fiber composites
LF	Aligned long fiber composites
MH	Modified Halpin-Tsai
E	Elastic modulus
E_c	Elastic modulus of composite
E_f	Elastic modulus of fiber
E_m	Elastic modulus of matrix
α	Randomness factor

l/d	Aspect ratio
V_f	Volume fraction
$E_{c,L}$	Elastic modulus of composite in the longitudinal direction
$E_{c,T}$	Elastic modulus of composite in the transverse direction

TABLE OF CONTENTS

	Page
ABSTRACT	iii
DEDICATION.....	v
ACKNOWLEDGEMENTS	vi
NOMENCLATURE	vii
TABLE OF CONTENTS	ix
LIST OF FIGURES.....	xi
LIST OF TABLES.....	xv
 1. INTRODUCTION.....	 1
1.1 Background	3
1.1.1 Cellulose Structure	3
1.1.2 Dispersion.....	6
1.1.3 Mechanical Reinforcement.....	8
1.1.4 Electric Field Alignment	11
1.2 Problem Statement	14
 2. EXPERIMENTAL.....	 18
2.1 Materials.....	18
2.1.1 Cellulose Extraction	19
2.2 Processing.....	21
2.2.1 Dispersion.....	21
2.2.1.1 Low Viscosity Silicone Oil.....	21
2.2.1.2 PVAc – Basic Method	21
2.2.1.3 PVAc – Modified Method	22
2.3 Electric Field Processing and Characterization.....	24
2.4 Characterization	26
2.4.1 Microscopy.....	26
2.4.2 Differential Scanning Calorimetry (DSC).....	26
2.4.3 Dielectric Spectroscopy.....	27
2.4.4 Dynamic Mechanical Analysis (DMA).....	28

2.4.5 Tensile Testing.....	29
2.4.6 Atomic Force Microscopy (AFM).....	31
2.4.7 Thermogravimetric Analysis (TGA)	31
3. RESULTS AND DISCUSSION	32
3.1 Dispersion.....	32
3.1.1 Silicone Oil.....	32
3.1.2 Basic Method - PVAc	33
3.1.3 Modified Method - PVAc	34
3.1.4 Comparison of Basic and Modified Methods	35
3.2 Electric Field Alignment	39
3.2.1 Cellulose Whiskers in Silicone Oil	39
3.2.2 Cellulose Whiskers in PVAc – Basic Method	45
3.2.3 Cellulose Whiskers in PVAc – Modified Method	51
3.3 Physical Properties	53
3.3.1 Differential Scanning Calorimetry	53
3.3.2 Water Absorption Study	55
3.3.3 Thermogravimetric Analysis	56
3.3.4 Dynamic Mechanical Analysis	57
3.3.4.1 Theoretical Predictions.....	62
3.3.5 Static Tensile Testing.....	69
4. CONCLUSIONS	81
4.1 Recommendations for Future Work	85
REFERENCES	86
APPENDIX	95
VITA.....	107

LIST OF FIGURES

FIGURE	Page
1.1 Schematic of (a) Hierarchical structure of cellulose and (b) Procedure to achieve MFCs (high shear mixing) and CWs (acid hydrolysis)	4
1.2 Transmission electron micrograph of cellulose whiskers obtained from acid hydrolysis of (a) microcrystalline cellulose, (b) tunicate, (c) cotton and (d) ramie	5
1.3 Transmission electron micrograph of cellulose microfibrils (a) bleached wood pulp, (b) cotton, (c) tunicin and (d) bacterial cellulose	6
1.4 DMA plot of tunicate cellulose whiskers reinforced latex system.....	9
1.5 DMA plot of Wheat straw cellulose whiskers reinforced latex system	9
1.6 Tensile stress vs strain plot of cellulose whiskers reinforced polymer nanocomposites	10
1.7 DMA plot of cellulose whiskers reinforced polyvinyl acetate	11
1.8 Alignment of native cellulose in chloroform and cyclohexane.....	12
1.9 AFM image of electric field oriented tunicate cellulose nanocrystals prepared at 10V with a frequency of 2.5×10^5 Hz and electrode width gap of 20 μ m.....	13
1.10 Potential application of AC electric field aligned CWs nanocomposites...	15
2.1 Extraction of CWs and MFCs from date palm tree.....	20
2.2 Flow chart showing the dispersion method.....	23
2.3 Picture of (a) Mold and (b) Aligned nanocomposite sample	24
2.4 Parallel electrode configuration setup. All dimensions are in mm.....	25
2.5 Curing profile used for the aligned nanocomposites.....	25
2.6 Profile of storage modulus as a function of temperature	29
2.7 Tensile test grips	30

2.8	Generic Stress Vs. Strain plot for polymers	30
3.1	OM images of (a) initial dispersion of CWs in acetone and (b) final dispersion of CWs in silicone oil	32
3.2	OM images of (a) Initial dispersion of CWs in acetone and (b) final dispersion of CWs in PVAc.....	33
3.3	SEM of fracture surface of 0.4wt% CWs/PVAc nanocomposite	34
3.4	AFM image of 0.4wt% CWs/PVAc nanocomposite	35
3.5	DSC of pure PVAc and CWs nanocomposites (a) basic method and (b) modified method.....	36
3.6	Stress Vs. strain plot of pure PVAc and CWs/PVAc composites with (a) Basic method and (b) Modified method	38
3.7	OM images of (a) before and (b) after electric field was applied	39
3.8	Effect of frequency and electric field on the alignment and chain formation of CWs in silicone. Scale bar in all the images is 100 μ m	41
3.9	Effect of time on the alignment and chain formation of CWs in silicone. Scale bar in all the images is 100 μ m.....	42
3.10	In-situ dielectric constant as a function of measurement frequency for (a) 500V _{pp} /mm and (b) 3000V _{pp} /mm.....	44
3.11	OM images of (a) random and (b) aligned CWs in PVAc at 100V _{pp} /mm, 1KHz for a duration of 20 minutes.....	46
3.12	Effect of frequency and electric field on the alignment and chain formation of CWs in PVAc. Scale bar in all the images is 100 μ m	47
3.13	Effect of time on the alignment and chain formation of CWs in PVAc. Scale bar in all the images is 100 μ m.....	48
3.14	In-situ dielectric constant as a function of measurement frequency for (a) 150V _{pp} /mm and (b) 500V _{pp} /mm.....	50
3.15	In-situ dielectric constant as a function of measurement frequency for (a) 100V _{pp} /mm and (b) 250V _{pp} /mm.....	52
3.16	DSC curves of aligned samples (a) 100V _{pp} /mm and (b) 250V _{pp} /mm	54

3.17	TGA curves of pure PVAc and CWs/PVAc nanocomposites	57
3.18	Storage modulus (parallel to alignment) as a function of temperature for 250V _{pp} /mm case	58
3.19	Storage modulus (parallel to alignment) as a function of temperature (below T _g) for 250V _{pp} /mm case	59
3.20	Storage modulus (perpendicular to alignment) as a function of temperature for 250V _{pp} /mm case	60
3.21	Storage modulus (perpendicular to alignment) as a function of temperature (below T _g) for 250V _{pp} /mm case.....	61
3.22	Experimentally measure modulus compared to theoretical prediction by Halpin-Tsai for randomly oriented composites.....	64
3.23	Comparison of experimental results (parallel to alignment) to rule of mixtures and Halpin-Tai predictions	66
3.24	Comparison of experimental results (perpendicular to alignment) to rule of mixtures and Halpin-Tai predictions.....	67
3.25	Comparison of experimental results (parallel and perpendicular to alignment direction) to rule of mixtures and Halpin-Tai predictions	68
3.26	Stress Vs. strain curves for pure PVAc, random and aligned cases (parallel to alignment direction) at room temperature	69
3.27	Initial portion of the stress Vs. strain curves for pure PVAc, random and aligned cases (parallel to alignment direction) at room temperature	70
3.28	Stress Vs. strain curves for pure PVAc, random and aligned cases (parallel to alignment direction) at 50°C.....	73
3.29	Initial portion of the stress Vs. strain curves for pure PVAc, random and aligned cases (parallel to alignment direction) at 50°C.....	73
3.30	Stress Vs. strain curves for pure PVAc, random and aligned cases (perpendicular to alignment direction) at room temperature	76
3.31	Initial portion of the stress Vs. strain curves for pure PVAc, random and aligned cases (perpendicular to alignment direction) at room temperature	76
A1	Storage modulus as a function of temperature	95

A2	Evolution of the (a) young's modulus (b) strength and (c) strain at break for PCL-based nanocomposites vs. filler (whisker or MFC)	97
A3	TEM of native cellulose oxidized for 5 minutes	100
A4	TEM of native cellulose oxidized for 60 minutes	100
A5	TEM of native cellulose oxidized for 120 minutes	101
A6	FTIR spectrum of MFCs (a) Non-oxidized and oxidized at different Time: (b) 5, (c) 60 and (d) 120 minutes	102
A7	FTIR spectrum of pristine CWs and oxidized CWs.....	102
A8	UV-Vis spectroscopy after 5 minutes oxidation as a function of number of cycles	103
A9	UV-Vis spectroscopy after 60 minutes oxidation as a function of number of cycles	104
A10	UV-Vis spectroscopy after 120 minutes oxidation as a function of number of cycles	105

LIST OF TABLES

TABLE	Page
2.1 Properties of DMF.....	18
2.2 Properties of PVAc	18
2.3 Properties of CWs	19
3.1 T_g results of pure PVAc and CWs/PVAc composites.....	37
3.2 T_g of aligned nanocomposites at $100V_{pp}/mm$ and $250V_{pp}/mm$	55
3.3 Weight change of pure PVAc and CWs nanocomposites before and after tensile testing.....	56
3.4 Storage modulus (parallel to alignment) as a function of temperature (below T_g) for $250V_{pp}/mm$	59
3.5 Storage modulus (perpendicular to alignment) of pure PVAc, random and aligned cases below T_g and comparison of percentage increase in E'	61
3.6 Elastic modulus of pure PVAc, random, and aligned cases at room temperature and comparison of percentage increase in elastic modulus....	71
3.7 Tensile strength and elongation at break for pure PVAc, random and aligned cases at room temperature	72
3.8 Elastic modulus of pure PVAc, random, and aligned cases at $50^\circ C$ and comparison of percentage increase in elastic modulus.....	74
3.9 Tensile strength and elongation at break for pure PVAc, random and aligned cases at $50^\circ C$	75
3.10 Elastic modulus of pure PVAc, random, and aligned cases (perpendicular to alignment) at room temperature and comparison of percentage increase in elastic modulus	78
3.11 Tensile strength and elongation at break for pure PVAc, random and aligned cases (perpendicular to alignment) at room temperature.....	79

3.12 Comparison of modulus enhancement we achieved with previous findings	80
A1 Mechanical properties of neat PU and prepared composites	96

1. INTRODUCTION

Cellulose is the world's most abundant, renewable, biodegradable polymer. Cellulose is known to occur in a wide variety of living species namely plants, animals, sea creatures, bacteria and algae [1]. Examples of plants that contain cellulose are flax, ramie, cotton, jute, sisal, hemp and palm [2]. In recent years cellulose based materials have attracted great interest in the plastic industry because of their low cost, recyclability, bio-compatibility, eco-friendliness, low density, ease of processability, high specific modulus and strength. Cellulose fiber reinforcements are showing a lot of promise in automotive applications [3-5]. Other potential applications like furniture, sports, aircrafts and railways are also being considered [6]. Also, cellulose has been known to be a piezoelectric polymer. Bazhenov first reported a piezoelectric response in wood [7]. In 1955, Fukada demonstrated that the observed piezoelectricity was due oriented cellulose crystallites [8]. Despite these early studies, cellulose as a smart material was not fully explored until recently. Researchers showed that cellulose based electro-active paper undergo large bending deformations when an electric field is applied [9-12]. Because cellulose is relatively cheap and biodegradable, it is advantageous for applications like smart skin, smart wall paper, MEMS, micro insect robots and so on [13-16].

This dissertation follows the style of *IEEE Transactions on Magnetics*.

In particular, cellulose whiskers (CWs) (obtained by chemical treatment of cellulose) as inclusions show a lot of promise that could address needs in multifunctional materials due to exceptional mechanical properties and their potential piezoelectric response [9, 17-19]. Since the first announcement of using CWs as a reinforcing phase [20-21], they have been extensively used as model fillers in several kinds of polymeric matrices, including synthetic and natural ones. A recent review reported the properties and application in nanocomposite field of cellulosic whiskers [1]. CWs occur as highly crystalline elongated rod-like particles or whiskers with aspect ratios ranging from 10-100. The precise physical dimensions of the crystallites depend on several factors, including the exact hydrolysis conditions, the ionic strength and particularly the source of cellulose. They can be as short as about a tenth of a micrometer, for cotton [22] and wood cellulose [23], or as long as several micrometers for tunicates or seaweeds such as *Valonia* [24]. The width is typically between 4 and 20 nm. On the other hand, Microfibrillated cellulose (MFC) consist of crystalline regions joined by amorphous regions. Like CWs, the dimensions depend on the source of cellulose. They are usually tens of microns in length and 50-100 nm in diameter. The properties of cellulose can potentially be exploited by using it as nanoscale reinforcement in polymers composites.

1.1 Background

1.1.1 Cellulose Structure

Native cellulose present in macroscopic fibers (plant fibers) consists of a hierarchical structure. The hierarchical structure is built up by smaller and mechanically stronger entities consisting of native cellulose fibrils. The fibrils interact strongly and aggregate to form native cellulose fibers [2]. These fibrils consist of crystalline regions connected by amorphous regions. The amorphous regions form weak spots along the fibril. These fibrils display high stiffness and are an ideal material for reinforcement of nanocomposite materials. The hierarchical structure is shown in Figure 1.1a. Figure 1.1b shows procedure used to prepare nanofillers from native cellulose.

There are various ways of preparing nanofibers from natural cellulose fibers. One such method consists of subjecting plant fibers to strong acid treatment combined with high power sonication. The acid treatment leads to hydrolysis of the amorphous regions, yielding rod-like nanofibers called cellulose whiskers. The acid hydrolysis leaves behind sulfate groups on the CWs. The electrostatic repulsion between the sulfate groups on the CWs help in dispersion of CWs in organic media. The dimensions of the cellulose whiskers depend on the source of the cellulose.

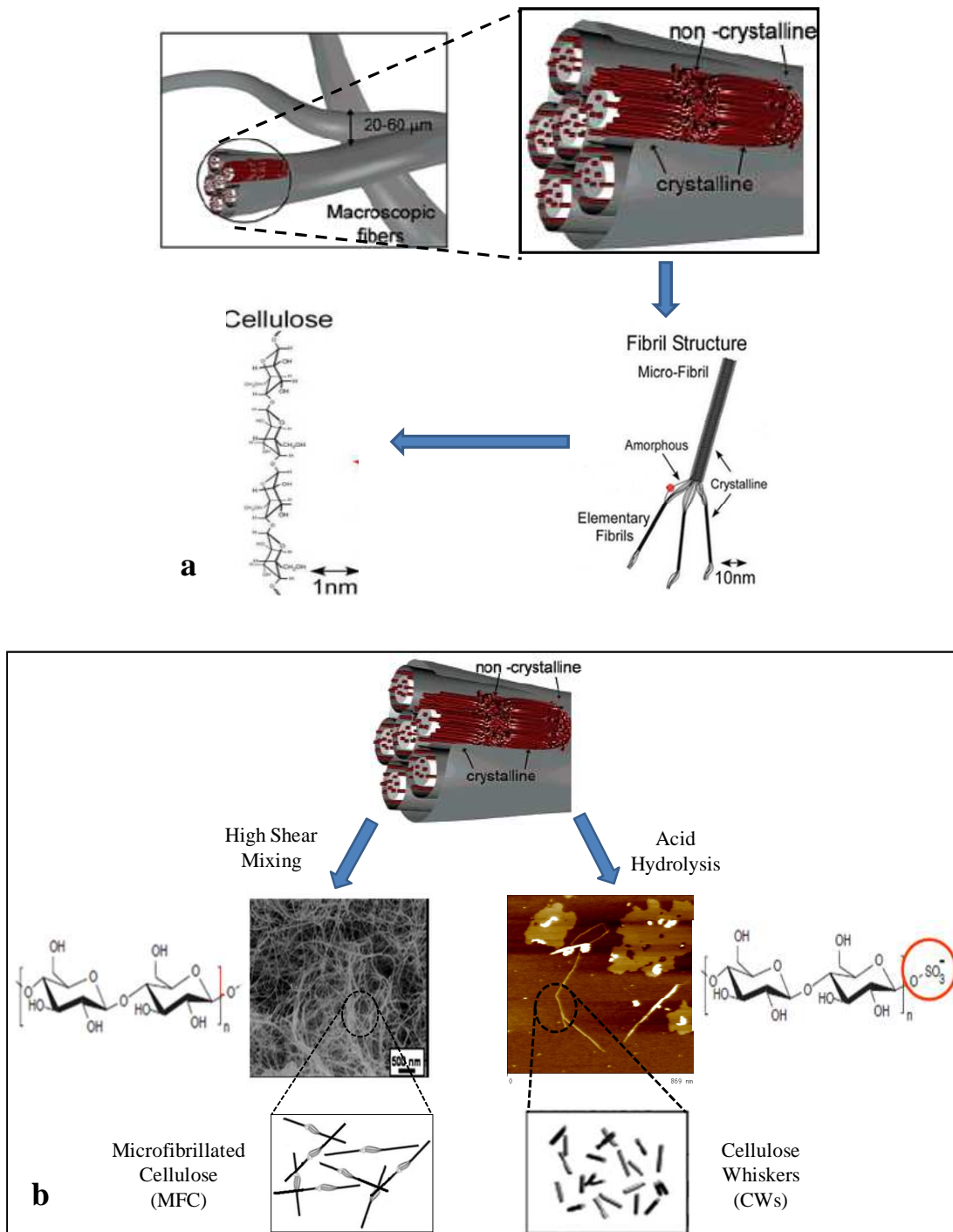


Figure 1.1: Schematic (a) Hierarchical structure of cellulose and (b) Procedure to achieve MFCs (High shear mixing) and CWs (acid hydrolysis) [25-26].

Some typical transmission electron microscope images of these CWs are shown in Figure 1.2.

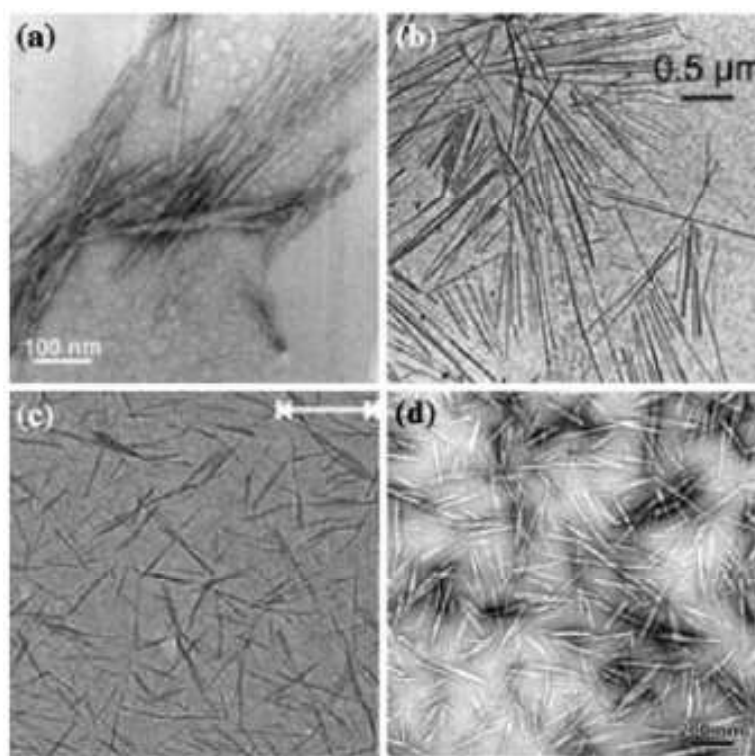


Figure 1.2: Transmission electron micrographs of cellulose whiskers obtained from acid hydrolysis of microcrystalline cellulose [27], b tunicate [28], c cotton [29], d ramie [30].

By excluding the hydrolysis step and subjecting the natural cellulose fibers to high mechanical shearing forces, breakdown of the fibers occurs, leading to a material called microfibrillated cellulose (MFC). The MFCs consist of both amorphous and

crystalline cellulose. Some typical transmission electron microscope images of MFCs are shown Figure 1.3.

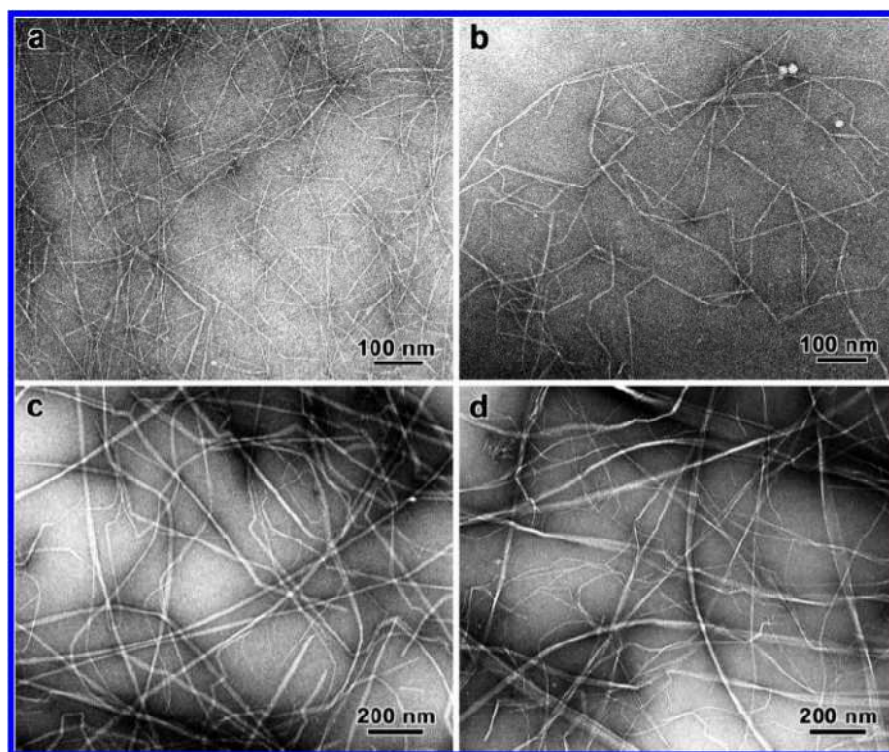


Figure 1.3: Transmission electron micrographs of cellulose microfibrils (a) bleached wood pulp, (b) cotton, (c) tunicin, and (d) bacterial cellulose [31].

1.1.2 Dispersion

CWs tend to agglomerate in bundles because of the tendency of whiskers to form strong hydrogen bonds with each other. Owing to agglomeration, the main concern associated with making effective nanocomposites from cellulose whiskers is dependent

on their homogeneous dispersion within a polymer matrix. Water is the preferred medium because of the high level of dispersion and high stability of cellulose whisker dispersions. Researchers have shown that excellent dispersion can be achieved in aqueous dispersed polymers, i.e., latexes, [20, 32-33]. Starting from the first study in 1995, the main focus in 90's (1995-1999) and early 2000's (2000-2005) was on reinforcing various water based polymers systems with high concentrations of various sources of CWs to achieve improvements in mechanical properties. There were 16 publications each in the 90's and early 2000's. However, this option restricts the choice of the matrix to water-soluble ones. To use CWs in non-aqueous systems they can be coated with a surfactant [34]. However, the high amount of surfactant needed to coat the high specific surface of CWs prohibits the use of this technique in composite applications. More recently (2006-2012), researchers have developed dispersion methods for use of CWs in non-water based polymer systems. There was renewed interest into looking at CWs for structural applications because of the new dispersion methods leading to 133 publications from 2006 to 2011. With the new dispersion methods, recently, it was shown that tunicin whiskers could be dispersed in DMF without additives or any surface modifications [35]. This result opens avenues for the use of CWs in non-water based polymer matrices.

1.1.3 Mechanical Reinforcement

Cellulose whiskers with different aspect ratios isolated from different sources, like tunicin [20], linter [36], cotton [37], straw [33], sisal [38], sugar beet [39] and MCC [40], were evaluated as a reinforcing phase in nanocomposites using different polymer matrices such as natural rubber, poly(styrene-co-butyl acrylate) [20, 32], PLA [36], PVA [40], POE [41-42] and PCL [43]. In most cases, the mechanical properties were substantially improved depending on the amount and homogeneity of cellulose filler dispersion. The strong reinforcing effect of the whiskers is generally attributed to the formation of a percolating network structure above the percolation threshold resulting from hydrogen bonding between nanoparticles [44-45].

CWs polymer nanocomposites have great potential in nanocomposite reinforcement applications. Since the first announcement of using cellulose whiskers as a reinforcing phase by Favier et al, new nanocomposite materials with original properties were obtained by physical incorporation of cellulose whiskers into a polymeric matrix [20, 33, 35, 46-48]. Favier et al. investigated the percolation of nanowhiskers extracted from tunicates [20] as shown in Figure 1.4. The authors measured shear modulus using the DMA. A spectacular improvement in the storage modulus after adding tunicin whiskers into a poly(S-co-BuA) matrix was observed. This increase was especially significant above the glass-rubber transition temperature. In the rubbery state of the thermoplastic matrix, the modulus of the composite with a loading level as low as 6 wt % is more than 2 orders of magnitude higher than the one of the unfilled matrix.

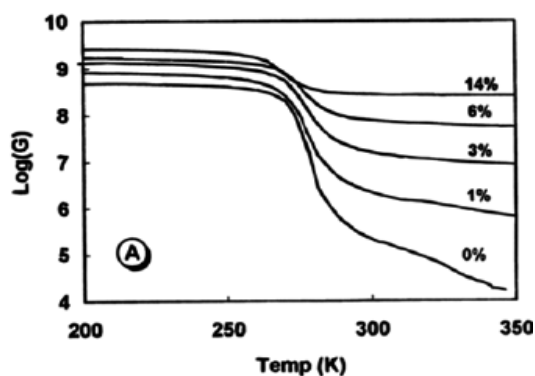


Figure 1.4: DMA plot of tunicate cellulose whiskers reinforced latex system [20].

Helbert et al. reported that a poly(S-co-BuA) latex film containing 30 wt% of wheat straw cellulose whiskers presented a rubbery Young's modulus value more than 1000-times higher than that of the bulk matrix [33] as shown in Figure 1.5. This effect was ascribed not only to the geometry and stiffness of the whiskers, but also to the formation of an H-bonded whiskers network.

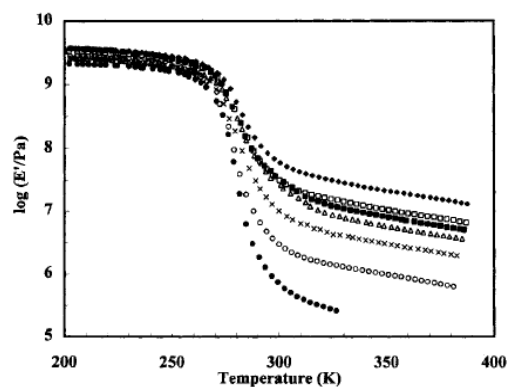


Figure 1.5: DMA plot of wheat straw cellulose whiskers reinforced latex system [33].

The enhancement in tensile modulus and strength of polymers, especially above T_g , is widely described in the literature [20, 30, 33]. However, the presence of whiskers tends to decrease the elongation at break of the nanocomposites compared to the neat matrix [1, 30, 49-50]. For example, Bendahou et al showed that with addition of 10wt% cellulose whiskers from palm trees to natural rubber, percent elongation decrease drastically from 576% to 16% (see Figure 1.6) [51].

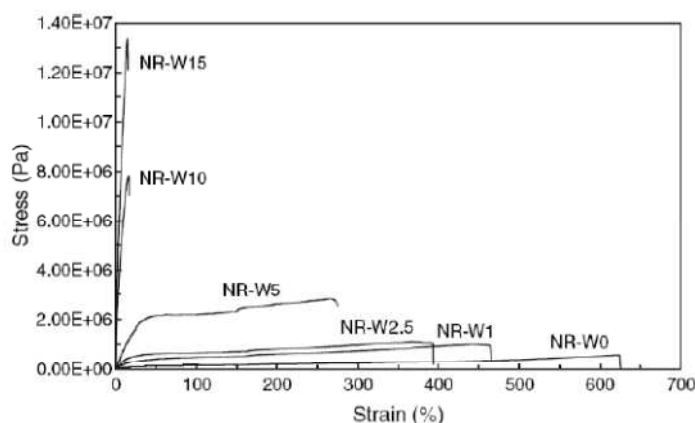


Figure 1.6: Tensile stress vs strain plot of cellulose whiskers reinforced polymer nanocomposites [51].

Most recently, Shanmuganatha et al used a solvent transfer method to make CWs reinforced polyvinyl acetate nanocomposites using an organic solvent [47]. The authors used 4 to 16.5wt% CWs in PVAc. The authors reported significant improvement in mechanical properties with the solvent transfer method as shown in Figure 1.7. They achieved a 100% and 4500% improvement in storage modulus below and above the T_g respectively.

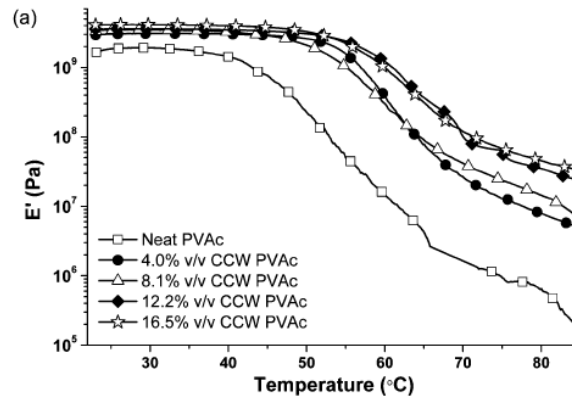


Figure 1.7: DMA of cellulose whiskers reinforced polyvinyl acetate [47].

To summarize, CWs reinforced composites showed significant improvement in mechanical properties. The drive for the significant improvement was attributed to the formation of 3D structure beyond the percolation threshold. Due to the strong hydrogen bonding, improvements as high as 5000% have been achieved. These improvements were typically achieved with high concentrations of CWs (10 wt% or more).

1.1.4 Electric Field Alignment

It has been shown that improvements in mechanical and electrical properties can be achieved by aligning nanoparticles in polymer nanocomposites [52-53]. Researchers have aligned various nanoparticles like SWNT [54-57], MWNT [58-59], gold [60] and CNF [61] in polymer nanocomposites.

Researchers have manipulated CWs in aqueous solutions under an external field using either shear forces [62] or magnetic fields [19]. However, there is limited work in the field of electric field - patterning of CWs in polymers. Bordel et al used AC electric field to align native cellulose in chloroform and cyclohexane [40]. They aligned native cellulose at 200V/mm and 1KHz alignment frequency and observed rotation of cellulose particles under electric field as shown in Figure 1.8. The study was limited to one AC electric field and frequency. Figure 1.8(a) shows random orientation and (b) shows aligned microstructure of native cellulose. The study did not make composites to study mechanical reinforcement.

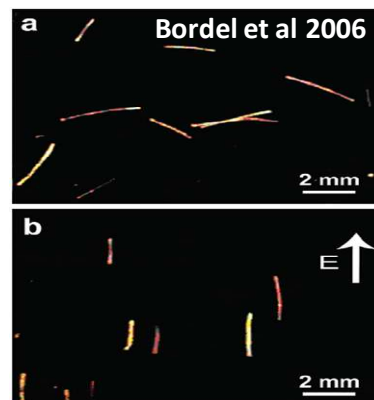


Figure 1.8: Alignment of native cellulose in chloroform and cyclohexane [40].

Habibi et al aligned cellulose nanocrystals using AC electric fields by varying the electric field and frequency to study the behavior of the cellulose nanocrystals in water using a surfactant [63]. They studied the behavior of cellulose for a wide range of voltages (2.5 – 20V/mm) for a frequency range of 1KHz to 2 MHz. Figure 1.9 shows the aligned microstructure they achieved. This study was also limited to alignment in

solution. In addition Bordel et al and Habibi et al used a parallel electrode configuration to carry out the experiments.

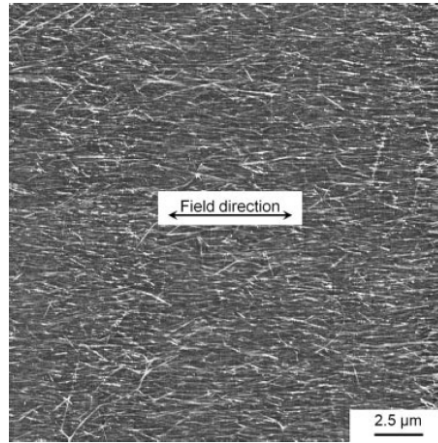


Figure 1.9: AFM image of electric field oriented tunicate cellulose nanocrystals prepared at 10 V with a frequency of 2.5×10^5 Hz and electrodes width gap of 20 μm [63].

In summary, a planar electrode configuration was used to carry out experiments reported in the literature. A planar electrode configuration is not amenable to processing of aligned CWs-reinforced polymer nanocomposites. Also, the effect of varying the frequency of the applied AC electric field for parallel electrode configuration has not been investigated before. Studying and understanding the change in microstructure by measuring in-situ dielectric properties was also not looked into.

1.2 Problem Statement

Some of the potential applications of AC electric aligned CWs nanocomposites are listed below in Figure 1.10. For example in battery applications PEO is used as a solid polymer electrolyte. The ideal operating temperatures of batteries are 50-80°C and PEO melts at ~50° C. Researchers have looked at reinforcing PEO with cellulose whiskers to improve the mechanical properties and thermal stability for battery applications. However, high concentrations of cellulose whiskers are needed to achieve improvements in elastic modulus and tensile strength. The high concentrations make the PEO brittle which is not ideal for battery application. Researchers have looked at reinforcing polymers with CWs for flexible display applications. By aligning low concentrations of CWs, we could potentially improve the elastic modulus and tensile strength by not detrimentally affecting toughness and elongation at break.

Similar to the problem in battery applications, significantly high concentrations were necessary to realize improvements. This usually affected the transparency and flexibility of the displays. By aligning low concentrations of CWs, we could potentially improve the elastic modulus and tensile strength by not detrimentally flexibility and transparency of the composites.

Cellulose is a piezoelectric polymer and has been shown to act as nucleating sites for polymer crystallization. Adding CWs to other piezoelectric polymer systems like PVDF and polyimides could potentially lead to improved piezoelectric response and by aligning CWs the mechanical properties can also be improved.

Finally aligned CWs can potentially be used in the packaging industry. Apart from improved mechanical properties, the aligned CWs microstructure will result in a torturous path for diffusion of gases leading to improved barrier properties.

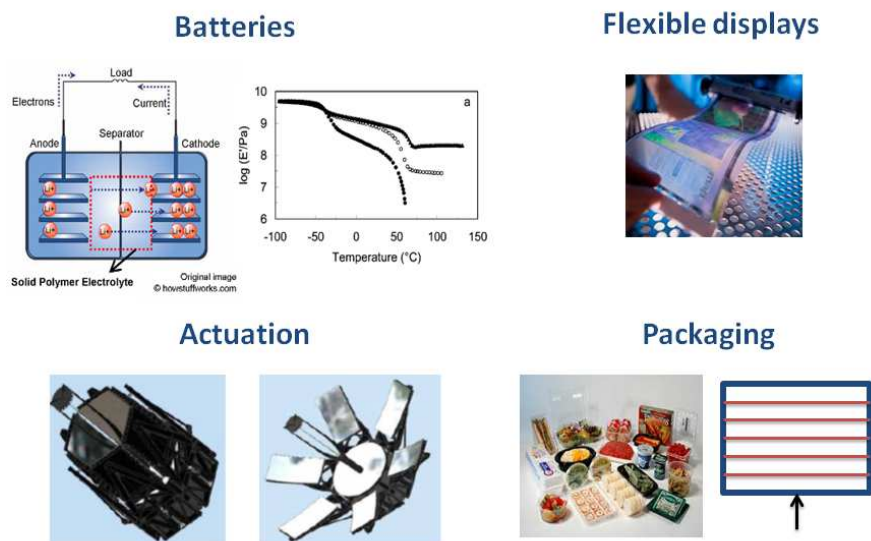


Figure 1.10: Potential applications of AC electric field aligned CWs nanocomposites.

This research targets a detailed investigation into the use of cellulose as reinforcing material in polymer nanocomposites by focusing on developing a methodology for dispersion and AC electric field alignment of cellulose based nanoparticles in polymer nanocomposites.

The purpose of this study is to investigate the assembly of CWs using an AC electric field as a function of electric field magnitude, frequency and duration for a parallel electrode configuration. Also, in the literature, researchers have used very high concentrations of CWs to realize improvements in storage modulus. This enhancement

in modulus is usually followed by a modest increase in strength but generally the ductility and toughness decrease. Our approach is to align small concentrations of CWs to achieve the kind of improvements reported in the literature by not detrimentally affecting toughness and ductility. The study will then be extended to preparing bulk PVAc composites with aligned CWs to access the effect of alignment on physical properties.

We propose to achieve our goals through the following steps;

i. Dispersion of CWs in polymer nanocomposites

In this step we will focus on developing a “processing method” wherein water can be removed by a solvent transfer method and replaced with a nonaqueous solution for cellulose whiskers dispersion in non water based polymer systems. We will then characterize the dispersion and relate results to state of dispersion.

ii. Electric field manipulation of micro CWs in polymer composites

We will firstly, align micron scale CWs to allow for visual inspection of the microstructure and to understand the behavior of CWs under an applied electric field and evaluate the effect of the following parameters;

- a) Electric field magnitude
- b) Frequency
- c) Duration of applied electric field

iii. Electric field manipulation of Nano CWs in polymer composites

With necessary understanding of the behavior of micro CWs, we will move on to aligning the nano scale dispersed CWs. We will develop a methodology that is amenable to composite processing with aligned cellulose and study the effect of AC electric field on the behavior of CWs in polymer composites and evaluate the above mentioned parameters.

iv. Exploring the impact on physical properties of aligned CWs reinforced polymer nanocomposites

In this step we investigate the effect of alignment on dielectric and mechanical reinforcement of CWs reinforced polymer nanocomposites. Specifically this includes the following tasks; firstly, characterize physical properties as a function of alignment parameters. Secondly compare the physical properties “parallel” and “perpendicular” to electric field direction to assess the enhancement in properties and finally understand the “mechanism” that drives the impact on physical properties.

2. EXPERIMENTAL

2.1 Materials

Acetone and Dimethylformamide (DMF) purchased from Sigma Aldrich were used as solvents to disperse. The properties of DMF are listed in Table 2.1. Polyvinyl acetate (PVAc) purchased from Sigma Aldrich was used as a model polymer. The properties of PVAc are listed in Table 2.2.

Table 2.1: Properties of DMF

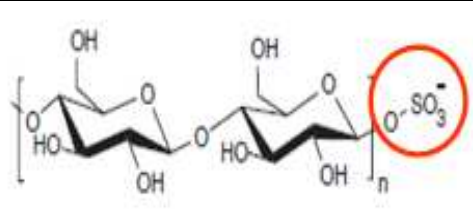
	DMF
Grade	Anhydrous
Evaporation temperature	60 °C
Density	0.944g/mL

Table 2.2: Properties of PVAc

	PVAc
Molecular weight	~100,000
T _g	42 °C
Density	1.18g/mL

CWs extracted from date palm trees were used (procedure is detailed below). The properties of CWs are listed in table 2.3.

Table 2.3: Properties of CWs

	CWs
Chemical Structure	
Functional Groups	Sulfate (SO_3^-) ~ 15%
Length	~260 nm
Diameter	~8 nm
Aspect ratio	~ 32

2.1.1 Cellulose Extraction

Cellulose whiskers and microfibrillated cellulose were extracted from the rachis of the date palm tree. Colloidal suspensions of CWs in water were prepared based on the method developed by, Wise, Marchessault and Paako. [25, 64-65]. A flowchart of the method used is shown in Figure 2.1. Fragments of the rachis of the palm tree were purified with a mixture of acetone /ethanol (68/32) using soxhlet. The purified matter

was twice submitted to alkali treatment with 2wt% of NaOH at 80°C for 2 hours and then subjected to four successive bleaching treatment using sodium chlorite (NaClO₂) 4,8 tampon solution at 70°C. The bleached pulp was then subjected to acid treatment with 65wt% sulphuric acid solution at 45°C for 45 min under stirring. Suspensions were washed with water until neutrality is reached, dialyzed against deionised water, and then filtered leaving behind CWs. On the other hand, the bleached pulp was subjected to high shear mixing to achieve MFCs

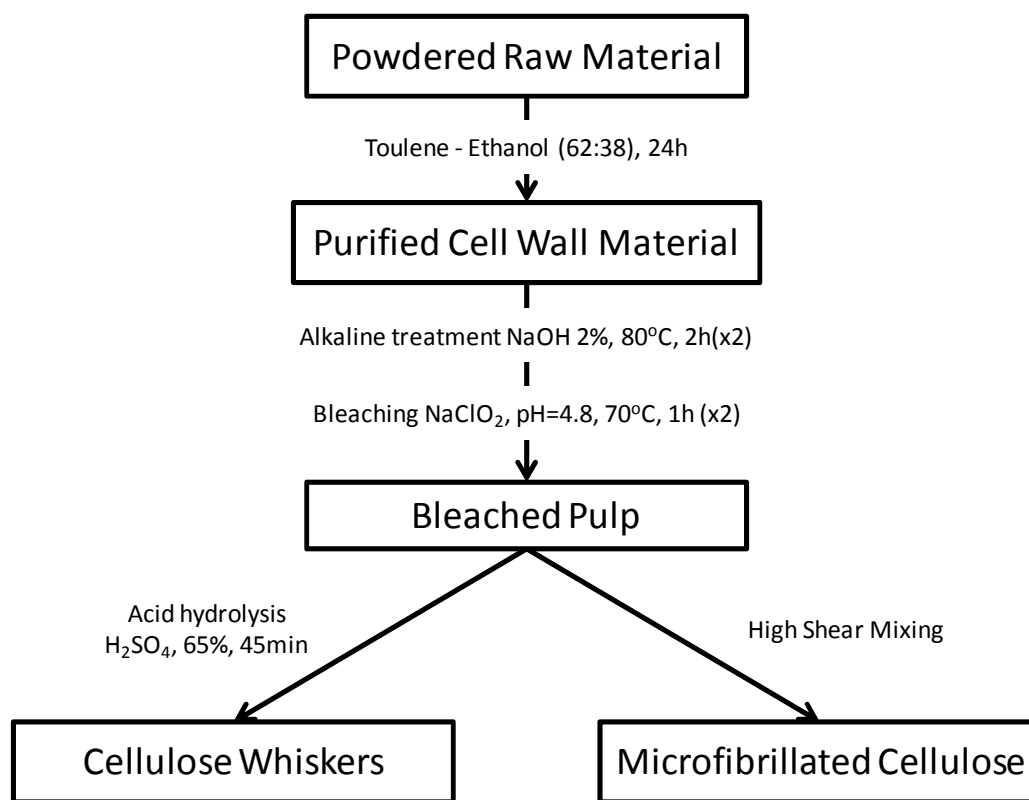


Figure 2.1: Extraction of CWs and MFCs from date palm tree.

2.2 Processing

2.2.1 Dispersion

2.2.1.1 Low Viscosity Silicone Oil

The extracted cellulose whiskers were dispersed in acetone under bath sonication. Weighed amount of silicone oil was then added to the solution. The solution was put on a hot plate at 60°C and stirred for 30 minutes at 150 rpm to enable the evaporation of acetone. The viscosity of the silicone oil used was 100cp.

2.2.1.2 PVAc – Basic Method

In this study we used a non-covalent approach to exfoliate the CWs. As received CWs (0.1g) were dispersed in 4 g of DMF under bath sonication for 4 hours. 1g of PVAc was dissolved in 4.9g DMF on a hot plate at 40°C separately. Both solutions were then mixed together, such that the final concentrations were 1, 10 and 89 wt% of CWs, PVAc and DMF respectively. The solution was then put in a bath sonicator and sonicated for an additional 4 hours. This solution was used for the In-situ alignment study to allow visual inspection of the microstructure and mechanism. This method will be referred to as the basic method.

Pure PVAc and CW/PVAc films were prepared by solution casting with the above described dispersion method. Films of pure, 0.1 and 0.2wt% CW/PVAc composites with 20wt% PVAc were cast. PVAc pellets were mixed with DMF as explained above. After the pellets dissolved completely in the solvent, the solution was poured onto a heat-resistant glass ceramic plate. A doctor blade was moved across the glass plate to create films of uniform thickness. The CW/PVAc micro-composites films were similarly cast with the following added steps; CWs were dispersed in DMF using a bath sonicator for 4 hours. The solution of dispersed CWs in DMF was then mixed with the PVAc/DMF solution and the mixture is further bath sonicated for 4 hours. The sonication times differ because at low concentration the CWs disperse easier than at high concentrations. This method was used to process the CW/PVAc composites. The thickness of the films were between 40-50 μ m.

2.2.1.3 PVAc – Modified Method

Due to the possibility of water (present in as-received CWs) acting as a plasticizer, a modified dispersion method was developed. A high power sonication method to exfoliate the CWs was used. A flowchart of the dispersion process is shown in Figure 2.2. As-received CWs (0.2g) were dispersed in 9.9 g of water under probe sonication for 10 minutes in an ice bath; the ice bath prevents evaporation of the solvent and degradation of the polymer. The solution was centrifuged at 8500 rpm for 15 minutes. The water was replaced by DMF and the solution is then sonicated for 10

minutes. This step is repeated five times to remove all the water present in the as-received CWs. The solution was then sonicated for an additional 60 minutes. 1g of PVAc was dissolved in 9.9g DMF on a hot plate at 40°C. Both solutions (CW-DMF and PVAc-DMF) were then mixed together, such that the final concentrations were 0.04, 10 and 89.96 wt% of CWs, PVAc and DMF respectively. The solution was then probe sonicated for an additional 60 minutes. This method will be referred to as the modified method.

CW/PVAc films were prepared by solution casting with the modified dispersion method to compare the mechanical properties achieved by the two dispersion methods.

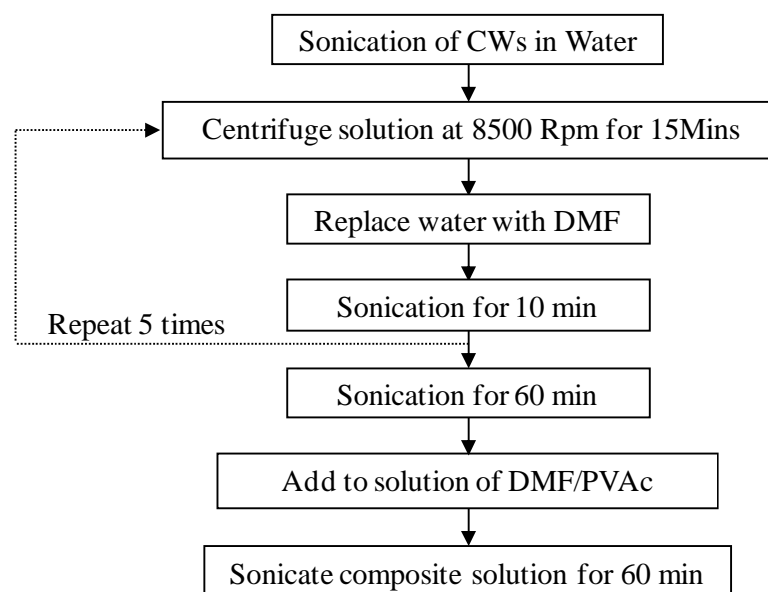


Figure 2.2: Flow chart showing the dispersion method.

A systematic study was done to figure out the power needed for the high power sonicator to achieve nanoscale dispersion. The ideal sonication parameters were found to

be 450 W power for 60 minutes of sonication time. Figure 2.3a and b show the mold used for study and aligned nanocomposite sample with dimensions.

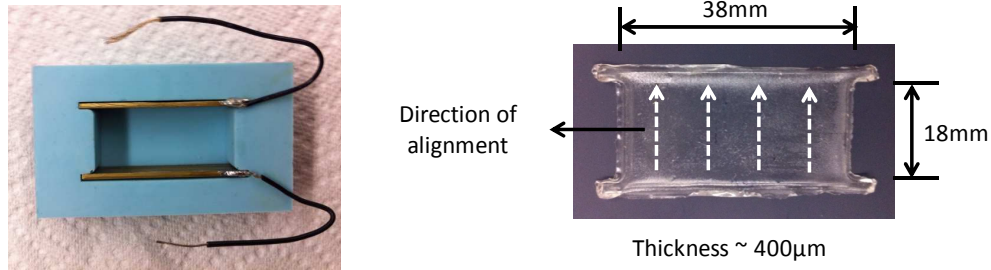


Figure 2.3: Picture of (a) Mold and (b) Aligned nanocomposite sample.

2.3 Electric Field Processing and Characterization

AC electric field was used to align and manipulate CWs in PVAc. Parallel electrodes separated by a distance of 1mm were used for the in-situ alignment study with the basic dispersion method. For making aligned nanocomposites parallel electrodes separated by 18mm were used as shown in Figure 2.4. An HP 33120A function generator supplied the AC voltages and this was integrated with a TREK 609D-6 high voltage amplifier. A variety of AC electric field magnitudes (100, 150, 200, 500 and 1000 V_{pp}/mm) were used for the in-situ study and (100, 150, 200 and 250 V/mm) for the aligned nanocomposite study. A wide range of frequencies (0.1 mHz to 1 MHz) were applied to the resulting solution for 20 minutes for the in-situ study and 1 Hour for the nanocomposite study.

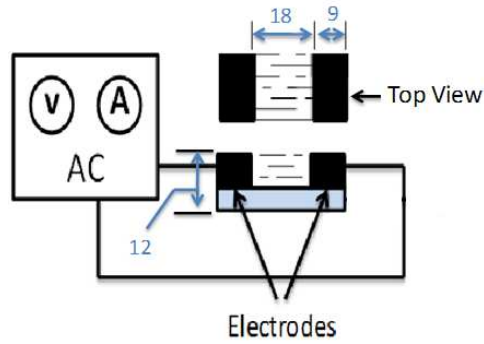


Figure 2.4: Parallel electrode configuration setup. All dimensions are in mm.

The 1 wt% CWs/ PVAc solution was poured in between the electrodes. AC electric field was applied for 1 hour. After 1 hour, the solution was heated to 60°C to evaporate the DMF. The temperature was maintained at 60°C and the electric field was left on for another 3 hours. The electric field was then switched off while the temperature was maintained for an additional 24 hours to remove any trapped DMF. Figure 2.5 shows the curing profile used. The sample was then removed from the mold and put in the vacuum oven to remove any residual DMF. The same electrode setup was used to measure in-situ dielectric properties.

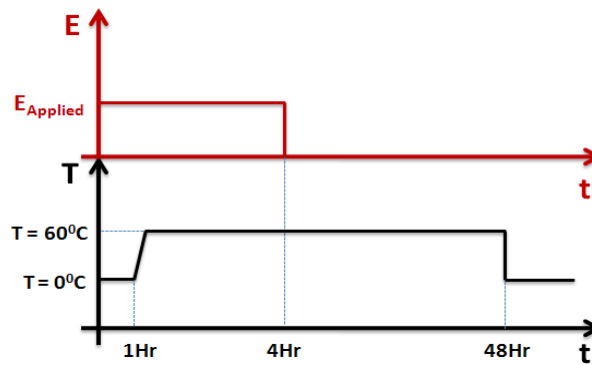


Figure 2.5: Curing profile used for the aligned nanocomposites.

2.4 Characterization

2.4.1 Microscopy

Optical Microscopy (OM) was used to characterize the dispersion and electric field effects on the CWs. OM images were obtained using a Zeiss Axiovert 200 Optical Microscope. Multiple OM images were taken of each film to assess uniformity throughout the film. Scanning Electron Microscope (SEM) images were obtained to study the CW dispersion. The CW/PVAc films were cleaned with isopropyl alcohol and then frozen in liquid nitrogen and fractured. Images of the fracture surface were obtained to better understand the dispersion of CWs. Transmission electron microscopy was used to study the effect of oxidation on the sizes of MFCs.

2.4.2 Differential Scanning Calorimetry (DSC)

DSC was used to investigate the behavior of the polymer with the addition of the CWs, using Q20 from TA instruments. For each measurement, a sample of about 10 ± 0.5 mg was placed in an aluminum pan and heated to 80°C at a heating rate of $10^{\circ}\text{C}\cdot\text{min}^{-1}$ and cooled to 0°C at the same rate. Data shown represent averages of at least three samples.

2.4.3 Dielectric Spectroscopy

The in-situ dielectric properties were used using a Quadtech[®] LCR meter. The measurements were done at room temperature at wide range of frequencies (50 Hz to 1 MHz). Data shown represent averages of at least three samples. The samples are electroded using high purity silver paint.

Dielectric broadband spectroscopy is used to measure the dielectric permittivity of the samples. A sinusoidal voltage in the form of $V=V_0 \sin(\omega t)$ is applied across the thickness of the sample and the current flow through the sample is measured by the instrument which is in the form of $I=I_0 \sin(\omega t+\delta)$. The ratio of output current to the input voltage is the complex capacitance of the material which can be written in the form of $C^*=C'+iC''$. Using parallel plate geometry the complex capacitance is converted to the complex dielectric permittivity of the material. Equation 1 shows the relation between capacitance and dielectric constant in parallel plate geometry setup:

$$C = \frac{\epsilon \epsilon_0 A}{d} \quad (1)$$

Where,

C = Capacitance

ϵ = Dielectric constant

ϵ_0 = Permittivity of free space

The capacitance of the aligned microstructure is measured from the LCR meter. Using equation 1 the dielectric constant of the aligned microstructure is calculated.

2.4.4 Dynamic Mechanical Analysis (DMA)

The dynamic mechanical properties of the nanocomposites were measured with a RSA III DMA from TA instruments. The tensile testing fixture was used at a frequency of 1Hz, a strain of 0.01%. A temperature range of -80°C to 80°C at a heating rate of 3°C/min was used. The tests were performed using samples with dimensions, approximately equal to 5 x 5 x 0.05 mm. Data shown represent averages of at least three samples.

In a DMA, an oscillatory strain in the form of $\varepsilon(t) = \varepsilon_0 \sin(\omega t)$ is applied to the sample where ε_0 is the strain amplitude, ω is the frequency, and t is time. For viscoelastic materials the dynamic stress (σ) can be expressed as:

$$\varepsilon(t) = \varepsilon_0 (E' \sin \omega t + E'' \cos \omega t) \quad (2)$$

Where E' and E'' are storage and loss moduli respectively. In addition, the ratio of loss modulus to storage modulus can be defined as the loss tangent: $\tan \delta = E''/E'$ where δ is called phase angle. Generic profile of storage modulus as function of temperature is shown in Figure 2.6.

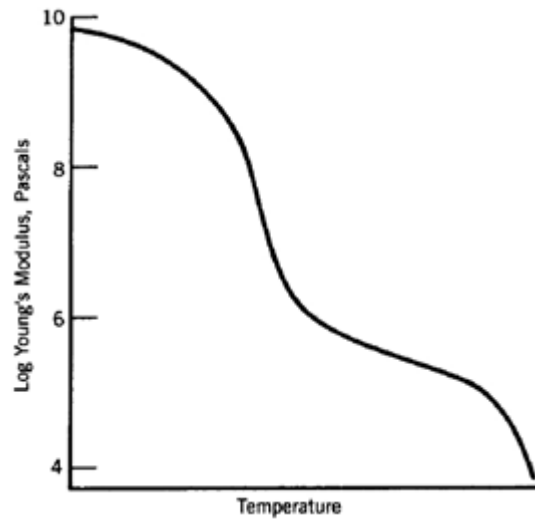


Figure 2.6: Profile of storage modulus as a function of temperature.

2.4.5 Tensile Testing

An Instron machine was used to perform the tensile tests on pure PVAc and composites made by the basic and modified method. These tests were performed using rectangular samples with dimensions; approximately equal to 40 x 5 x 0.05 mm. Tensile tests were also performed on the aligned samples and compared to pure PVAc and randomly oriented composites. These tests were performed using rectangular samples with dimensions of 8 x 5 x 0.4 mm. Data shown represent averages of at least three samples. The grips used are shown in Figure 2.7.

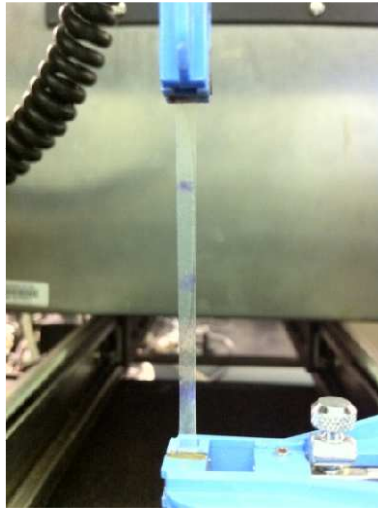


Figure 2.7: Tensile test grips.

Figure 2.8 shows the generic stress vs. strain plot for polymers. The slope of the linear portion of the stress-strain curve is used to measure the elastic modulus (E) of the material. The maximum stress is taken to be the tensile strength (TS). The area under the stress-strain gives the toughness of the material and finally the maximum length to which the material can extend is the percentage elongation (% EL).

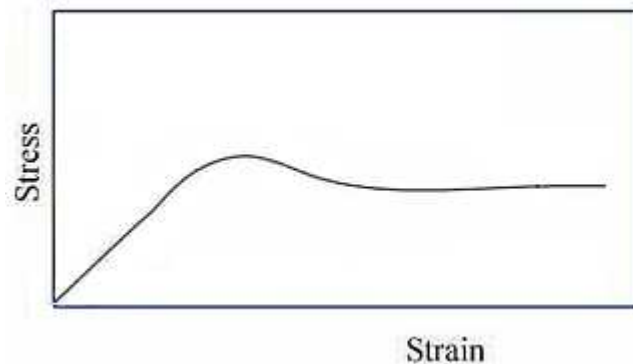


Figure 2.8: Generic Stress Vs. strain plot for polymers.

2.4.6 Atomic Force Microscopy (AFM)

A Bruker Icon AFM was used to study the dispersion as well as CWs sizes. The AFM was used in the scanning mode. The tip of the AFM is scanned laterally across the surface and the vertical movements of the tip are recorded. This information is used to construct a quantitative 3D image of the surface. Surface AFM was done of the random samples to study the dispersion of CWs in PVAc and cryogenically fractured samples were used to study the alignment of CWs in PVAc.

2.4.7 Thermogravimetric Analysis (TGA)

Presence of moisture and solvent in the nanocomposites were measure using a TGA from TA instruments. Presence of moisture and solvent content can be measured by the changes in weight of the samples with increasing temperature. The heating cycle used for this study was 30°C to 250°C at a heating rate of 10°C per minute. Samples of 10-15mg were used for the study.

3. RESULTS AND DISCUSSION

3.1 Dispersion

3.1.1 Silicone Oil

Method described in chapter 2 section 2.2.1.1 was followed to disperse CWs in silicone oil. Important features of silicone oil are included in Table 2.1 of chapter 2. The sonication process helps prevent reagglomeration of CWs in addition to breaking the large CW agglomeration. OM images showed CWs were dispersed as small bundles ($< 50\mu\text{m}$) and not as individual whiskers, resulting in a microcomposite. However, there is a possibility that a few of the CWs were individually dispersed; due to the resolution of the OM, it is not possible to verify if that is the case. Figure 3.1a shows the pre-dispersion of CWs in acetone and Figure 3.1b shows the final dispersion of CWs in silicone oil. The dispersion of CWs was found to be stable over long periods of time.

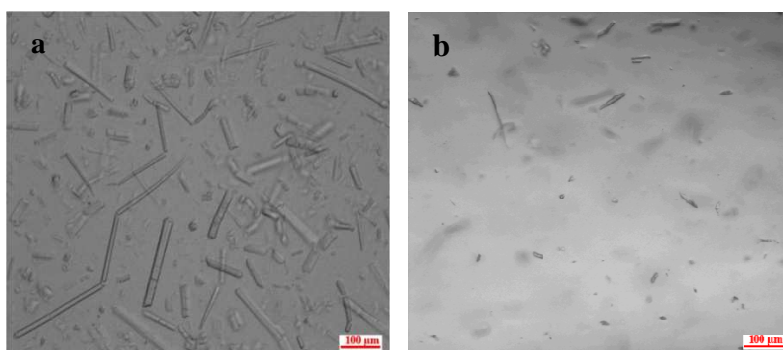


Figure 3.1: OM images of (a) Initial dispersion of CWs in acetone and (b) final dispersion of CWs in silicone oil.

3.1.2 Basic Method - PVAc

The OM of as-received CWs in acetone is shown in Figure 3.2a. By ultrasonating the CWs in acetone and then dispersing them in PVAc a homogeneous dispersion of CWs results as shown in Figure 3.2b. The detailed procedure followed is given in chapter 2 section 2.2.1.2. The sonication process significantly reduces the large CWs agglomeration. Although CWs were homogeneously dispersed, optical images (OMs) show that they were dispersed as small bundles ($< 10\mu\text{m}$) and not as individual whiskers, resulting in a microcomposite (Figure 3.2b). However, it is possible that a few of the CWs were individually dispersed. Owing to the resolution of the OM, it is not possible to see them if that is the case.

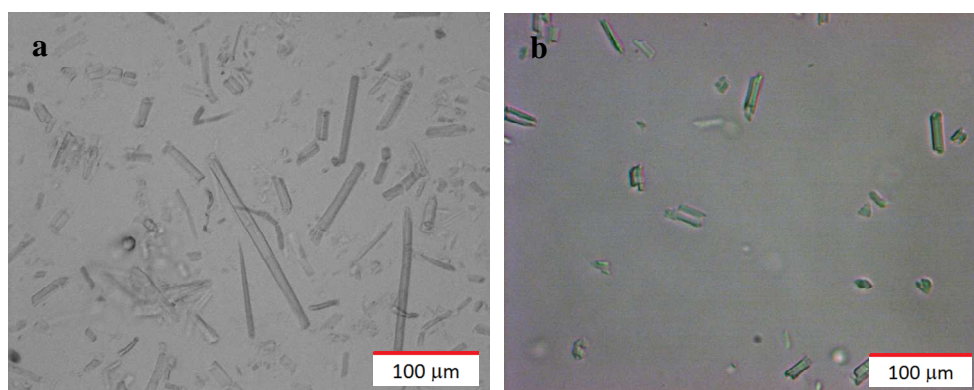


Figure 3.2: OM images of (a) Initial dispersion of CWs in acetone and (b) final dispersion of CWs in PVAc.

3.1.3 Modified Method - PVAc

Method described in chapter 2 section 2.2.1.3 was followed to disperse CWs in PVAc. The high power sonication method leads to homogeneous dispersion of CWs in PVAc. Figure 3.3 shows the SEM image of the fractured surface of 0.4wt% CWs/PVAc nanocomposite. CWs were individually dispersed with average lengths and diameters of ~260 nm and ~8 nm respectively yielding an aspect ratio of approximately 33.

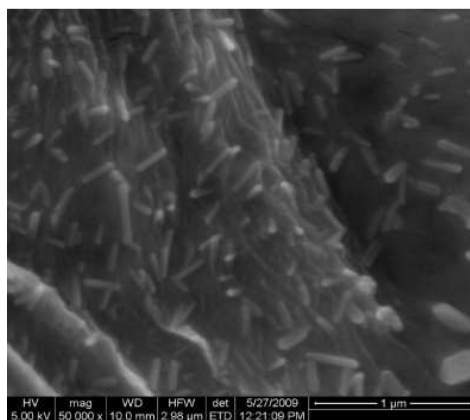


Figure 3.3: SEM of fracture surface of 0.4wt% CWs/PVAc nanocomposite.

AFM was used to further verify the sizes of CWs in PVAc. Figure 3.4 shows an AFM image of surface of 0.4wt% CWs/PVAc nanocomposite. The average dimensions of the CWs were found to be ~260nm in length and ~8nm in width as evidenced by SEM. The dimensions of CWs from the above SEM and AFM were compared to the AFM image of as received CWs in PVAc. It was found that the dimensions of as received CWs in water and CWs dispersed were found to be the same.

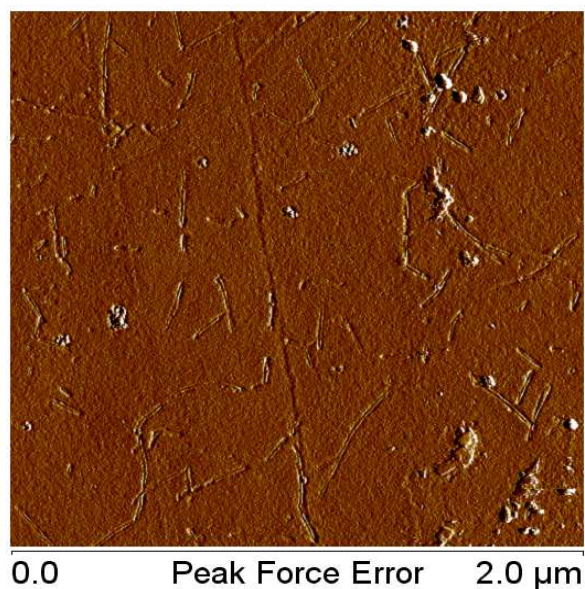


Figure 3.4: AFM image of 0.4wt% CWs/PVAc nanocomposite.

3.1.4 Comparison of Basic and Modified Methods

DSC was used to study the thermal behavior of the polymer and the CWs reinforced polymer composites. Figure 3.5 and Table 3.1 shows the DSC results of pure PVAc and CW/PVAc composites processed using the basic and modified methods. No melting or re-crystallization peaks were observed. This behavior is typical of an amorphous polymer. The glass transition (T_g) temperature of PVAc was found to be 42 ± 0.4 °C. The T_g of 0.1wt% and 0.2wt% CW/PVAc (basic method) were found to be 40 ± 0.12 °C and 39 ± 0.15 °C. This is due to the water present in as received CWs. However, with the modified method the T_g of 0.1 and 0.2wt% CWs/PVAc composites is

42°C. No change is the T_g of the polymer confirms that water was completely removed by the modified method.

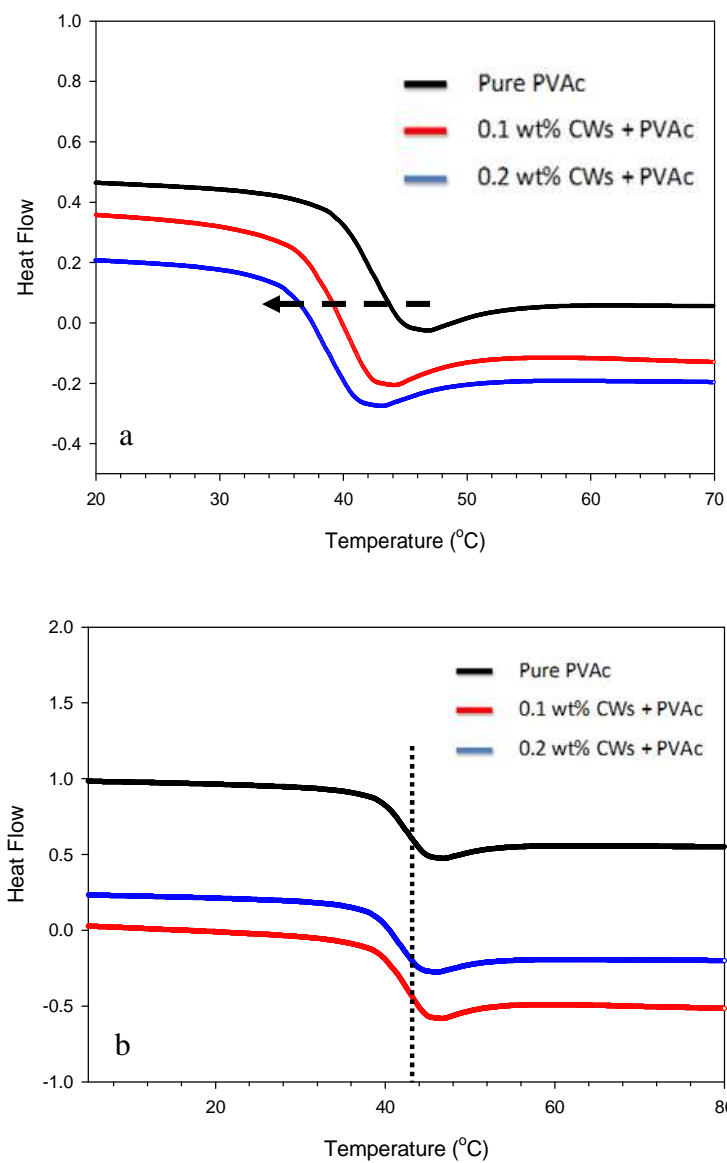


Figure 3.5: DSC of pure PVAc and CWs nanocomposite (a) basic method and (b) modified method.

Table 3.1: T_g results of pure PVAc and CW/PVAc composites

Sample	T_g (basic method)	T_g (modified method)
Pure PVAc	$42 \pm 0.4^\circ\text{C}$	$42 \pm 0.06^\circ\text{C}$
0.1wt% CWs + PVAc	$40 \pm 0.12^\circ\text{C}$	$42 \pm 0.13^\circ\text{C}$
0.2wt% CWs + PVAc	$39 \pm 0.15^\circ\text{C}$	$42 \pm 0.23^\circ\text{C}$

Tensile tests were performed on samples (as described in chapter 2 section 2.4.5) to investigate the effect of CWs reinforcement in CW/PVAc composites with the basic and modified methods. Figure 3.6 shows the stress-strain plots of pure PVAc and CW/PVAc composites. The elastic modulus of pure PVAc (calculated from the slope of the linear region of stress-strain curve) was found to be 10 MPa as shown in the inset. With the basic method, the elastic moduli of 0.1wt% and 0.2wt% CW/PVAc composites drop to 5 and 4 MPa respectively. It seems the reduction in elastic modulus is due to the water present in as received CWs acting as a plasticizer. With the modified method, the elastic moduli increase to 14 ± 1.17 and 15 ± 1.21 MPa for 0.1 and 0.2wt% CWs/PVAc composites.

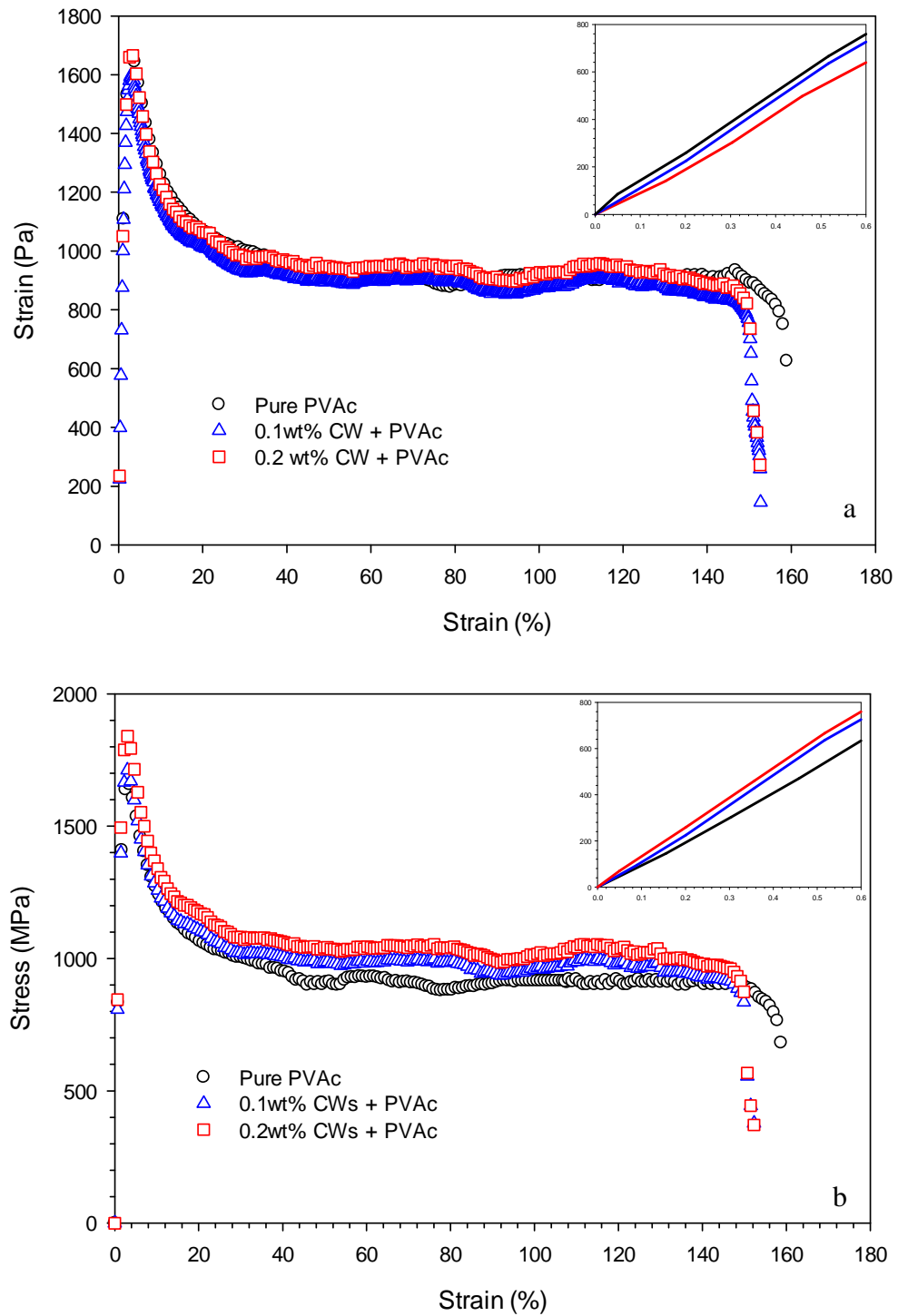


Figure 3.6: Stress vs. Strain plot of pure PVAc and CW/PVAc composites with (a) basic method and (b) modified method.

3.2 Electric Field Alignment

3.2.1 Cellulose Whiskers in Silicone oil

Solution of 1wt% CWs dispersed in silicone oil was used as described in chapter 2 section 2.2.1.1. AC electric fields of 500, 1000, 2000 and 3000V_{pp}/mm were applied at varying frequency (1mHz to 100KHz). OM images were taken before and after the electric field was applied as shown in Figure 3.7. Figure 3.7a shows the CWs randomly dispersed with no preferred orientation. Figure 3.7b shows OM images at 500V_{pp}/mm. The change in the microstructure due to the applied electric field is a two step process: Firstly the CWs rotate in the direction of the electric field for all applied frequencies as shown in Figure 3.7b.

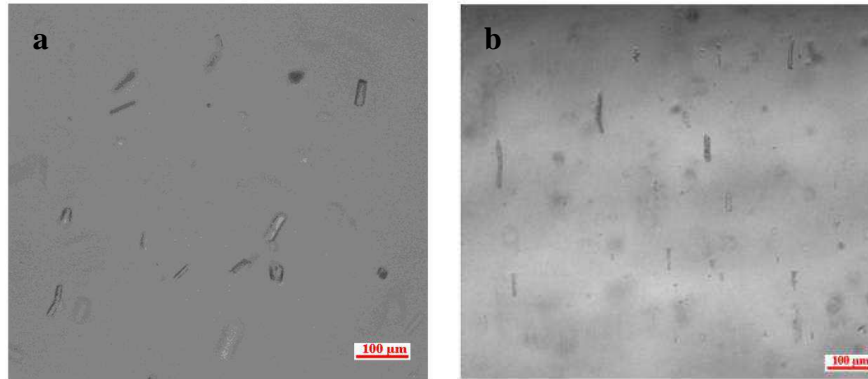


Figure 3.7: OM images of (a) before and (b) after electric field was applied.

The second step involves the formation of chains as shown in Figure 3.7: at a low frequency range of 1 mHz – 100 mHz, thin chains of CWs were observed. At 500 mHz frequency, very good alignment and chain formation were achieved. Between 1Hz and 1

kHz, CWs do align in the direction of electric field but form thinner chains as compared to 500 mHz. For frequencies higher than 1 KHz, some CWs align in the direction of the electric field but no chain formation was observed. Based on these findings, 500 mHz was found to be the optimal frequency for both alignment and chain formation. The behavior described above was consistent for all electric fields. As the electric field was increased from $500V_{pp}/mm$ to $3000V_{pp}/mm$, the thickness of the chains significantly increased. Figure 3.8 shows the effect of frequency and electric field on the alignment and chain formation of CWs. In general, chain formation was dependent on the frequency indicating that the driving force is dielectrophoresis. Dielectrophoretic force arises from a non uniform electric field. In this work, a uniform AC electric field was applied to the CW/Silicone oil solution. Contrast in the dielectric constants of CWs and silicone oil distorts the uniform electric field lines resulting in a non uniform local electric field [18]. The gradient in the electric field causes the CW bundles to experience a dielectrophoretic force. Dielectrophoretic force acts on the polarized CW bundles and due to their polarization, the CWs bundles are attracted to the regions of higher electric field intensity. This leads to the formation of CW chains. The dielectrophoretic force is a function of the Clausius Mossoti factor, where the Clausius Mossoti factor is dependent on the dielectric constant of the CWs and silicone oil and is therefore dependent on the frequency. As a result, the dielectrophoretic force changes as the frequency of alignment is varied.

It was also observed that the alignment and chain formation were dependent on time as shown in Figure 3.9. From 0 to 5 minutes, the particles start rotating in the

direction of the electric field. Very thin chains start to form at 10 minutes and these chains become thicker as the field is left on.

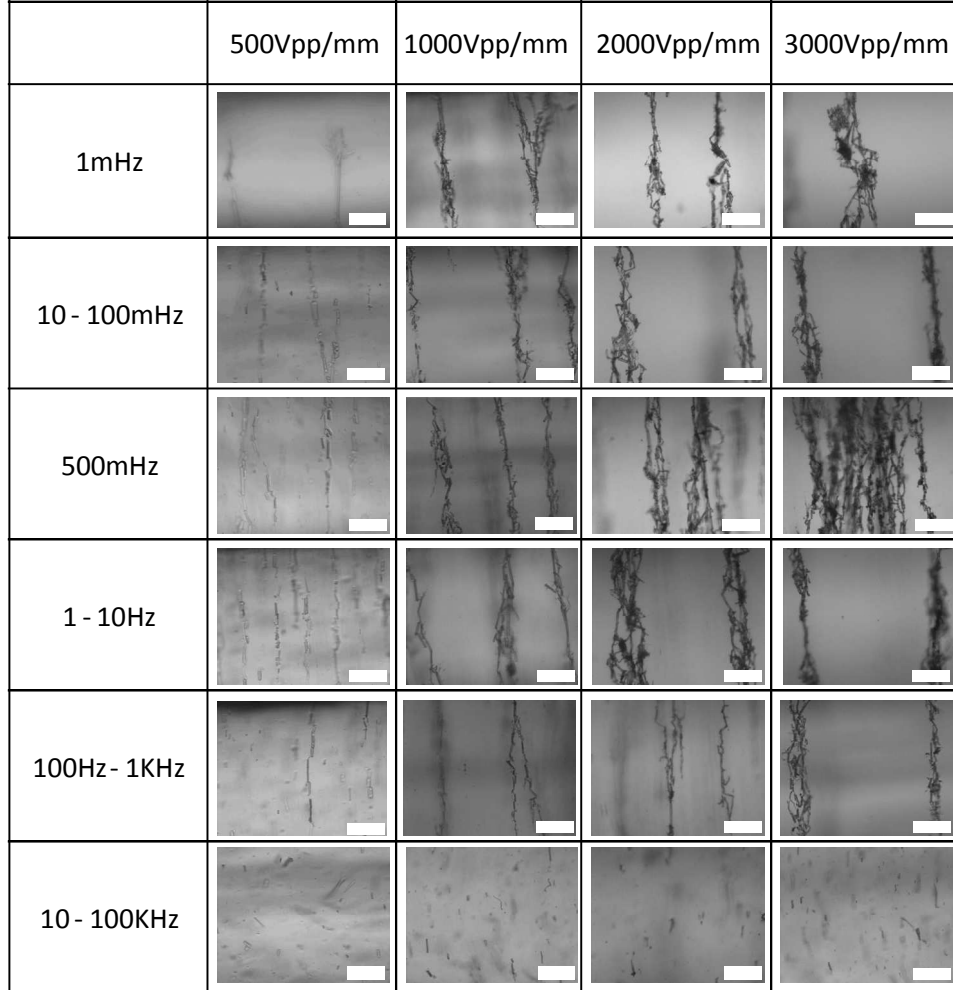


Figure 3.8: Effect of frequency and electric field on the alignment and chain formation of CWs in silicone oil. Scale bar in all the images is 100 μ m.

The gap between the chains also increases. Beyond 10 minutes, the alignment and chain formation continues until 20 minutes for all frequencies and electric fields. At

the end of 20 minutes there were very thick and highly dense chains. The thick chains are comprised of many thin chains. Beyond 20 minutes no further improvement in alignment or chain formation was visually observed under the microscope. Therefore, alignment duration of 20 minutes was selected as optimum. We characterized the solutions by measuring the dielectric properties to verify that there was no improvement in alignment and chain formation beyond that point.

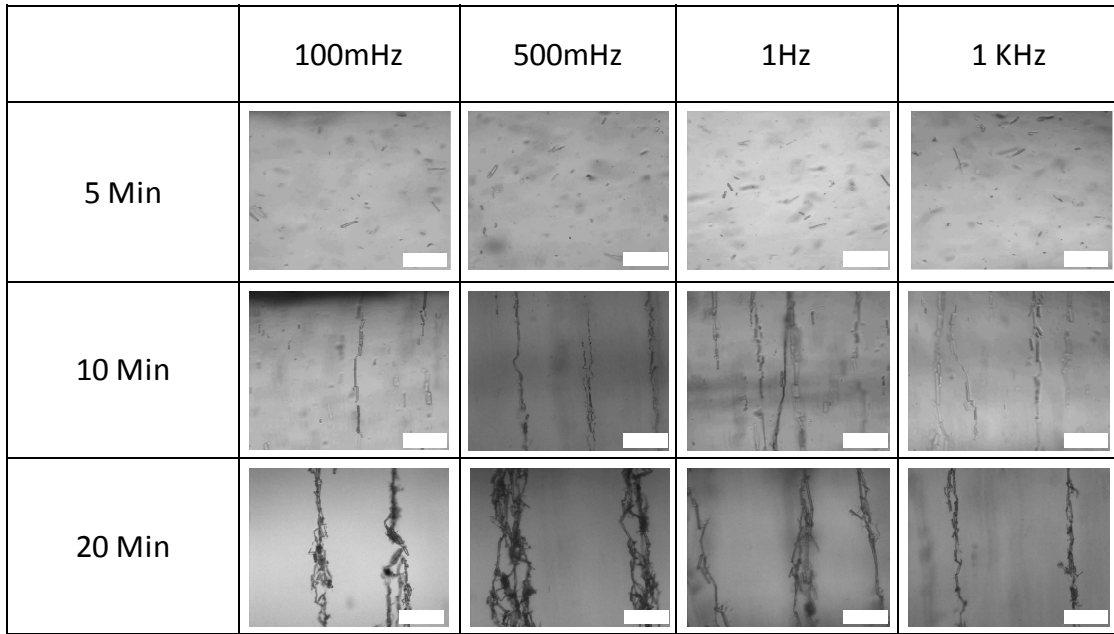


Figure 3.9: Effect of time on the alignment and chain formation of CWs at 1000 V_{pp}/mm at different alignment frequencies. Scale bar in all the images is 100 μm .

In-situ dielectric properties of the solutions were measured while the electric field was on to gauge the extent of alignment and its impact on effective properties. The dielectric constant is measured in the same direction as alignment. The measurements

were made in the liquid state after applying an electric field at two magnitudes (500 V_{pp}/mm and 3000 V_{pp}/mm) for 20 minutes for a wide range of alignment frequency (0.1 mHz – 100 KHz). At each alignment frequency case, the dielectric constant was measured as a function of input measurement frequency, from 50 Hz to 1 MHz. The result is shown in Figure 3.10a (500 V_{pp}/mm alignment field) and Figure 3.10b (3000 V_{pp}/mm alignment field). For all cases, the dielectric constant of the solution showed a dependence on the measurement frequency. Herein, the ‘random case’ refers to the solution with dispersed CWS prior to alignment by AC field. For the random case, the dielectric constant starts at about 9 at 50 Hz (measurement frequency) and settles to a value of ~ 7 at 1 MHz (Figure 3.10a). For the aligned cases at 500 V_{pp}/mm (also Figure 3.10a), the dielectric constant value increases as compared to the random case, reaching values between 14 (at the lower measurement frequencies) to 12 (at 1 MHz). In general, at this electric field magnitude, alignment frequency does not seem to affect the final value of dielectric constant. This behavior is consistent with the observed morphology shown in Figure 3.8. Alignment and thin chain formation in all these alignment cases at 500 V_{pp}/mm yield a similar microstructure, and therefore result in similar effective dielectric constant. At 3000 V_{pp}/mm (Figure 3.10b), significant improvement in dielectric constant was observed with some values reaching 20, and there is a noticeable difference in dielectric constant for different alignment frequencies as compared to the random case. At 10 mHz alignment frequency, the dielectric constant increases from 9 for the random case to ~ 16 .

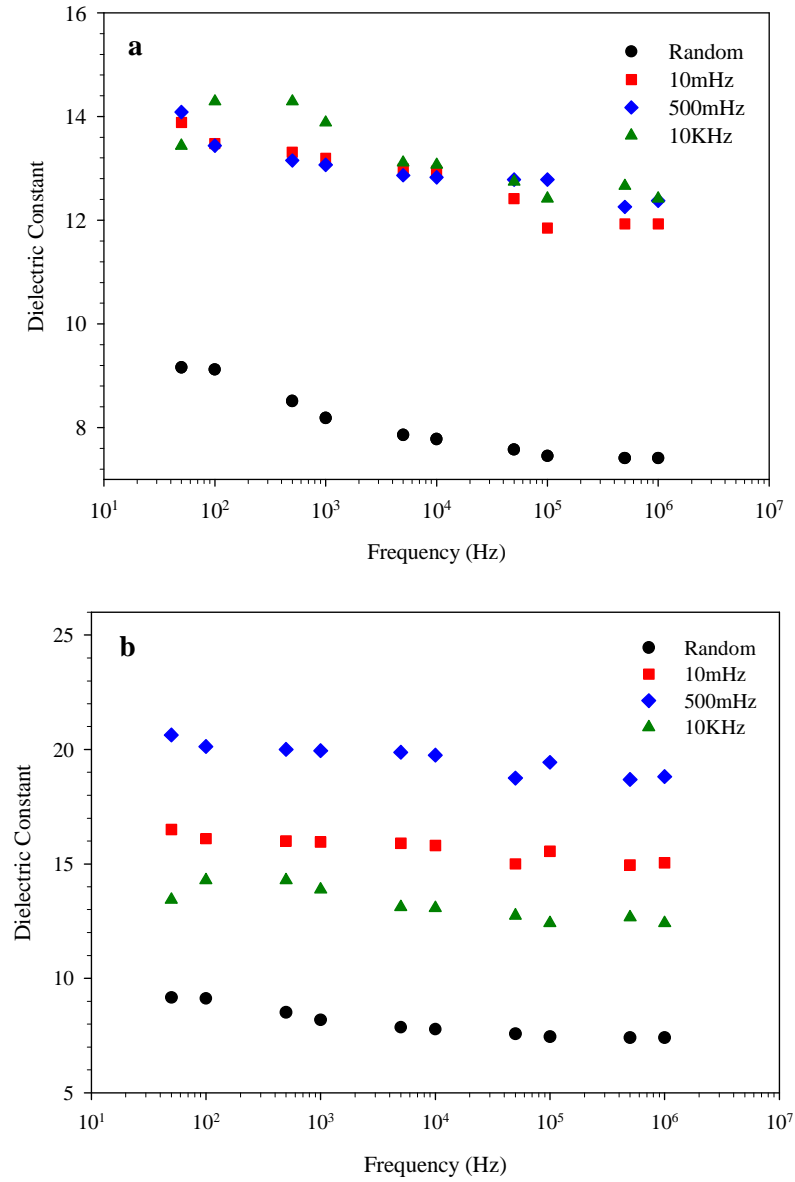


Figure 3.10: In-situ dielectric constant as a function of measurement frequency for (a) 500 V_{pp}/mm and (b) 3000 V_{pp}/mm.

When the alignment frequency is increased to 500 mHz, the dielectric constant increases further to ~20. Finally, when the alignment frequency is 10 KHz, the dielectric constant value drops to ~14, although still higher than the random case. Once again, the

dielectric constant behavior parallels the aligned microstructures seen in Figure 3.8 for the 3000 V_{pp}/mm case, further confirming that the CWs were well aligned and chain formation bridging between both surfaces is having an impact on the effective properties.

3.2.2 Cellulose Whiskers in PVAc – Basic Method

Solution of 1wt% CWs dispersed in PVAc was used as described in chapter 2 section 2.2.1.2. AC electric fields of 100, 150, 200, and 1000 V_{pp}/mm were applied at varying frequencies (100 Hz to 1 MHz). Figure 3.11a shows OM images of the random case. Herein, the ‘random case’ refers to the solution with dispersed CWs prior to alignment by AC field. Figure 3.11b shows the OM after an electric field of 100 V_{pp}/mm was applied for 20 minutes. The CWs response to the applied electric field is a two step process: First, the CWs rotate in the direction of the electric field. Second, the ends of the CWs bundles interact with each other and form long chains in the direction of the electric field. Finally the chains interact with each other to form thicker chains. The degree of alignment of CWs in PVAc was dependent on the alignment frequency, electric field magnitude and time.

At low alignment frequency of 100 Hz, most of the CWs rotate in the direction of the electric field. This behavior was observed for all electric fields at this frequency. At alignment frequencies of 1, 10 and 50 KHz, both rotation and chain formation were observed for 100, 150 and 200 V_{pp}/mm (Figure 3.12).

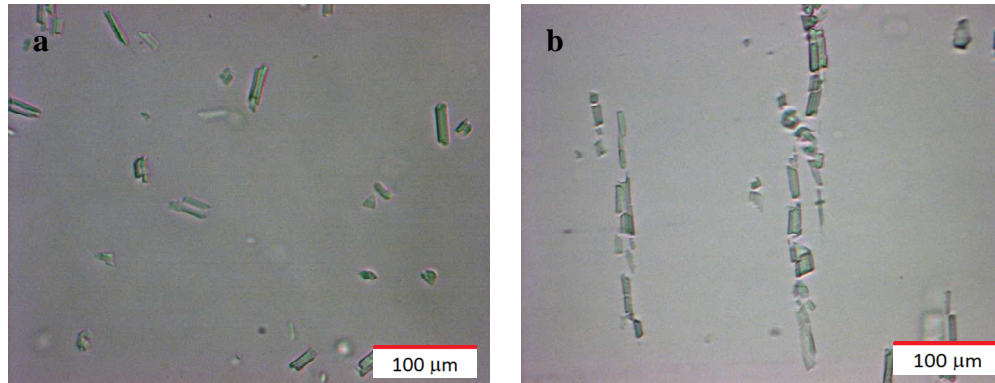


Figure 3.11: OM images of (a) Random and (b) Aligned CWs in PVAc at $100V_{pp}/mm$ and 1 KHz for a duration of 20 minutes.

After rotation and chain formation the CWs chains start to interact with each other to form thicker chains as a function of time. At 500 and 1000 V_{pp}/mm , only short chains formation was observed, and therefore they do not cross from one electrode to the other. At 100 KHz alignment frequency, CWs rotate in the direction of the electric field but no chain formation was observed; this behavior was observed for all electric fields. We are interested in both rotation and chain formation because the previous study in oil showed impact on dielectric properties was highest when chains formed and connected across the electrodes.

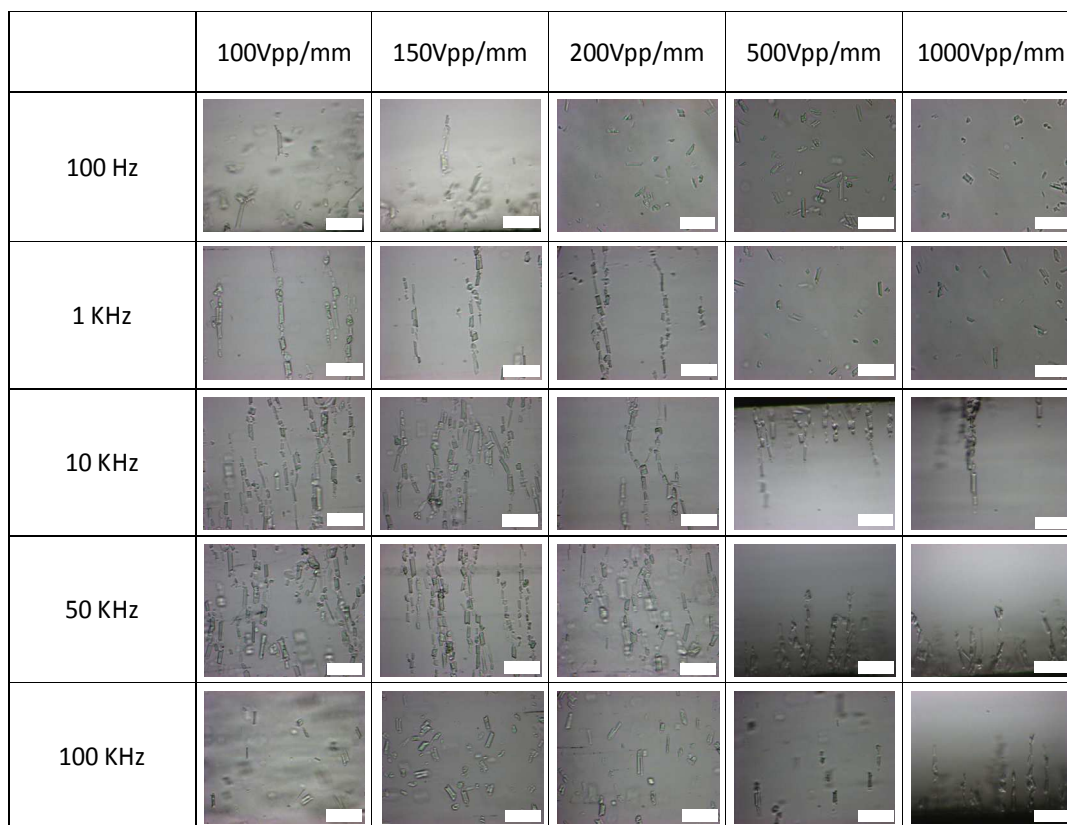


Figure 3.12: Effect of frequency and electric field on alignment and chain formation of CWs. Scale in all images is 100 μ m.

It was also observed that the alignment and chain formation were dependent on time as shown in Figure 3.13. From 0 to 1 minutes, the particles start rotating in the direction of the electric field. Very thin chains start to form at 5 minutes and these chains become thicker as the field is left on. Beyond 10 minutes, the alignment and chain formation continues until 20 minutes for all frequencies and electric fields. At the end of 20 minutes there were thick and dense chains. The thick chains are comprised of many thin chains. Beyond 20 minutes no further improvement in alignment or chain formation

was visually observed under the microscope. Therefore, alignment duration of 20 minutes was selected as optimum. We characterized the solutions by measuring the dielectric properties to verify that there was no improvement in alignment and chain formation beyond that point.

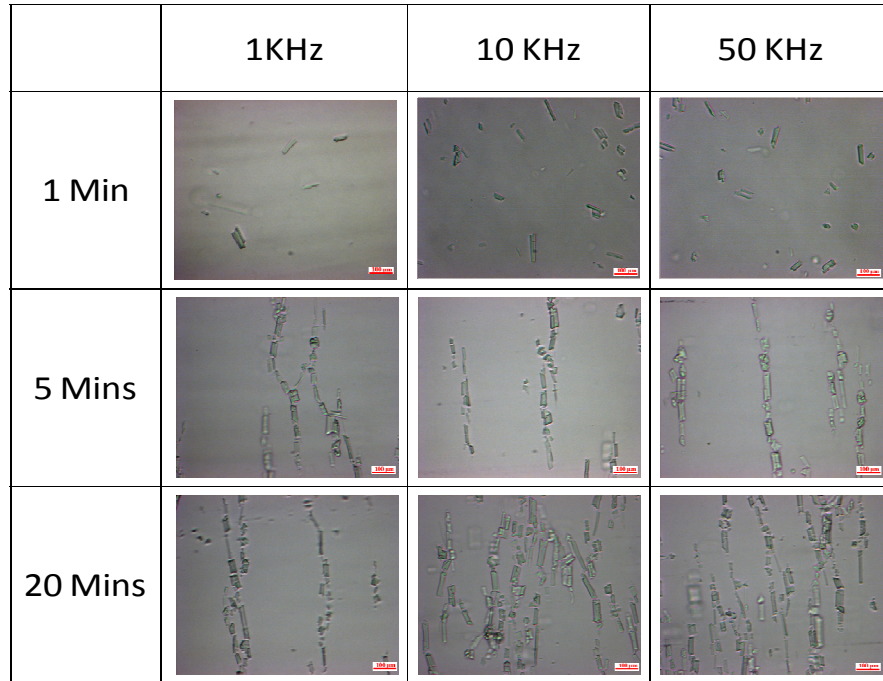


Figure 3.13: Effect of time on alignment and chain formation of CWs. Scale in all images is 100 μ m.

To show the impact of alignment and chain formation on the dielectric properties, dielectric constant as a function of measurement frequency for 150 and 500 V_{pp}/mm was measured as shown in Figure 3.14a and b. The dielectric constant before and after the AC electric field was applied showed a dependence on the measurement frequency.

Dielectric constant of the solution without applying the AC electric field was found to be 9 at low and 7 at high measurement frequency. At 500 V_{pp}/mm (Figure 3.14a), improvements in dielectric constant for various alignment frequencies as compared to the random case were observed. For alignment frequencies of 1, 10 and 100 KHz the dielectric constant hovers around 10-12. However, there was no significant difference in the dielectric constant at different alignment frequencies for this electric field. This behavior is consistent with the alignment and chain formation that were achieved for 500 V_{pp}/mm as seen in Figure 3.12. For 150 V_{pp}/mm (Figure 3.14b), significant improvements in dielectric constant were observed as compared to the random case. In addition, the dielectric constant was higher at 50 KHz as compared to the 1 KHz and 100 KHz alignment cases, mirroring the alignment behavior shown in Figure 3.12. Optimum properties were achieved at 50 KHz for duration of 20 minutes for field magnitudes ranging from 100-200 V_{pp}/mm , as seen optically and in terms of enhancement in dielectric properties. This set of parameters is hence taken as the favorable alignment conditions.

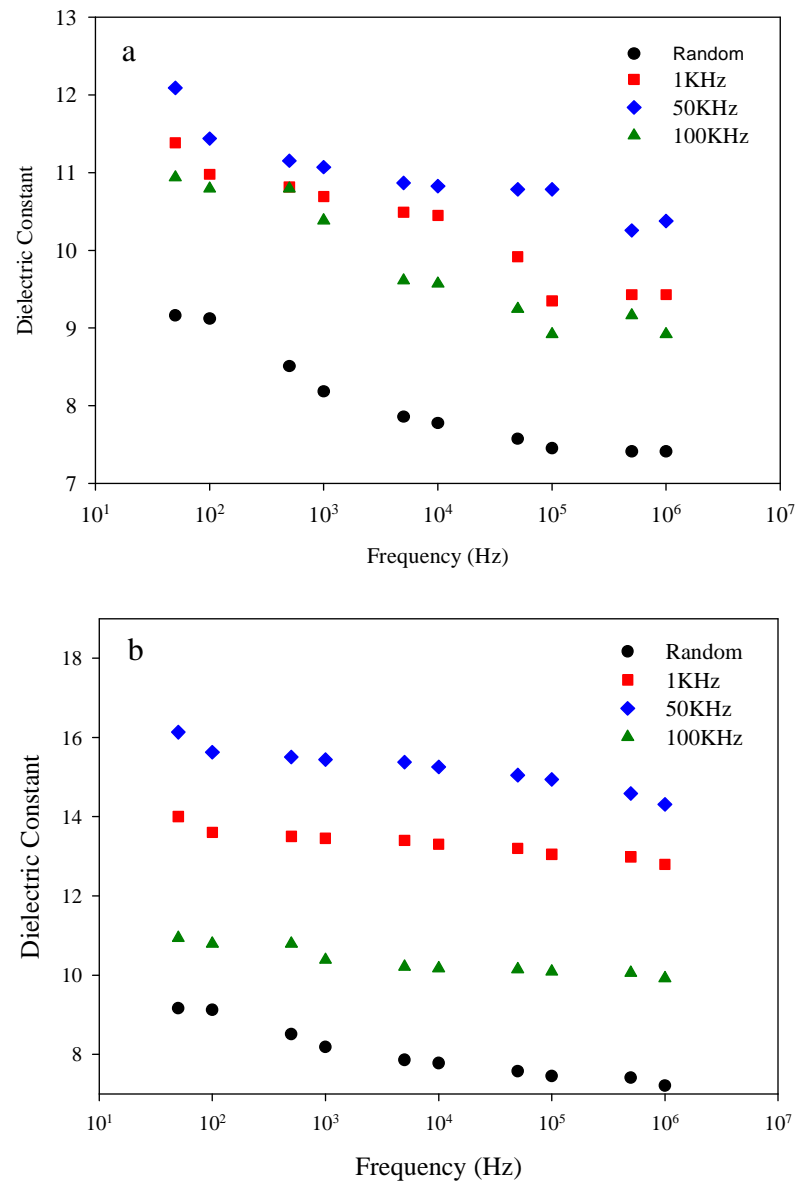


Figure 3.14: In-situ dielectric constant as a function of measurement frequency for (a) 150 V/mm and (b) 500 V/mm.

3.2.3 Cellulose Whiskers in PVAc – Modified Method

With the necessary understanding of the behavior of micro CWs we move on to the alignment of individually dispersed CWs in PVAc. Since the CWs were dispersed in the nanoscale in-situ alignment was no longer possible. Hence we used in-situ dielectric properties as a tool to gauge the alignment of CWs as a function of alignment parameters. In-situ dielectric constant measurements were done after applying the electric field for 4 hours to assess the effect of alignment parameters on the microstructure of CWs reinforced nanocomposite solutions. Figure 3.15a and b shows the dielectric constant as a function of measurement frequency at $100V_{pp}/mm$ and $250V_{pp}/mm$ respectively. For the random case, the dielectric constant starts at about 9 at 50 Hz (measurement frequency) and settles to a value of ~ 7 at 1 MHz (Figure 3.15a), a behavior typical of a dielectric material. For all the aligned cases at $100V_{pp}/mm$ (also Figure 3.15a), the dielectric constant value is close to the random case. In general, at this electric field magnitude, alignment frequency does not seem to affect the final value of dielectric constant. At $250V_{pp}/mm$ (Figure 3.15b), increase in dielectric constant was observed with some values reaching 11, and there is a slight difference in dielectric constant for different alignment frequencies as compared to the random case. At 1Hz alignment frequency, the dielectric constant increases from 9 for the random case to 9.5. When the alignment frequency is increased to 10Hz, 100Hz and 1 KHz the dielectric constant increases to 10.5, 10.7 and 10.8. There seems to be a trend wherein the change in microstructure is causing an increase in dielectric constant. This behavior was

observed in our previous study wherein the alignment and chain formation of micro CWs in PVAc was the driving force for an increase in dielectric constant [17].

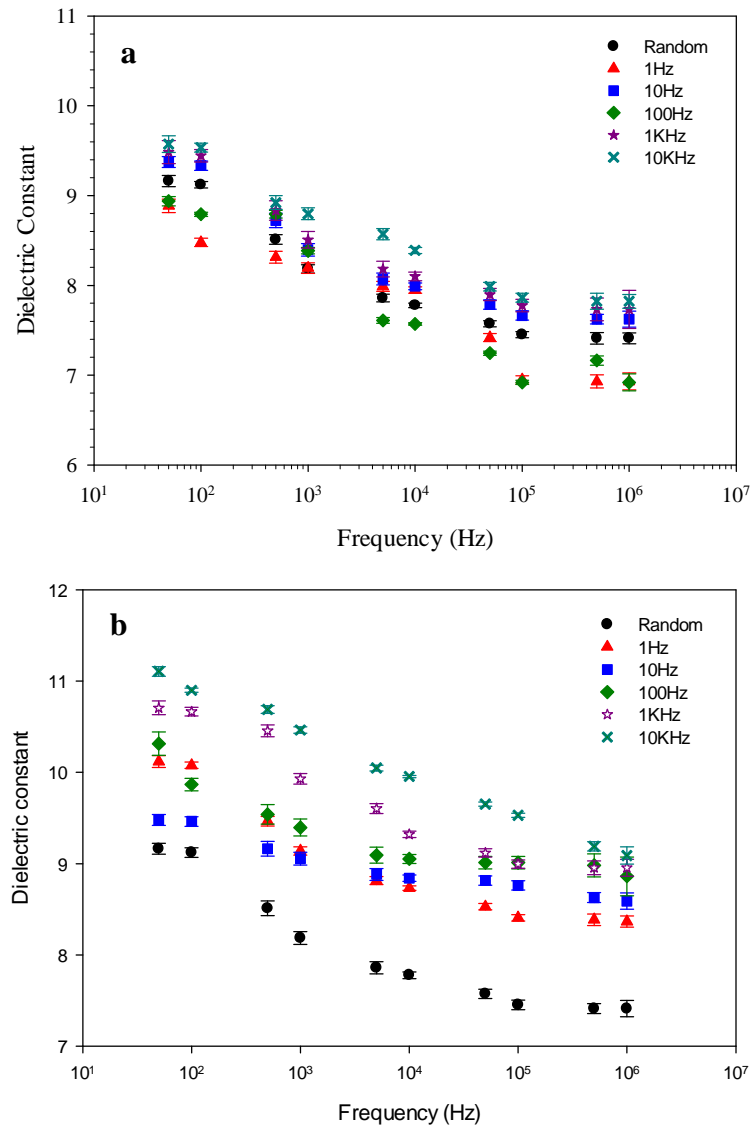


Figure 3.15: In-situ dielectric constant as a function of measurement frequency at (a) 100V_{pp}/mm and (b) 250 V_{pp}/mm.

This trend observed in dielectric constant with alignment frequency is indicative of a change in microstructure with alignment of CWs occurring in the 250V_{pp}/mm case as compared to the 100V_{pp}/mm case.

3.3 Physical Properties

3.3.1 Differential Scanning Calorimetry

Figure 3.16a and b and Table 3.2 show the DSC curves for nanocomposites aligned at 100V/mm and 250V/mm. The T_g was found to be $\sim 42 \pm 0.13^\circ\text{C}$. DSC results showed no effect on T_g for aligned composites as compared to pure PVAc and randomly oriented nanocomposites. The alignment does not affect the long range molecular motion of polymer chains. DSC results show that water present in CWs was completely removed.

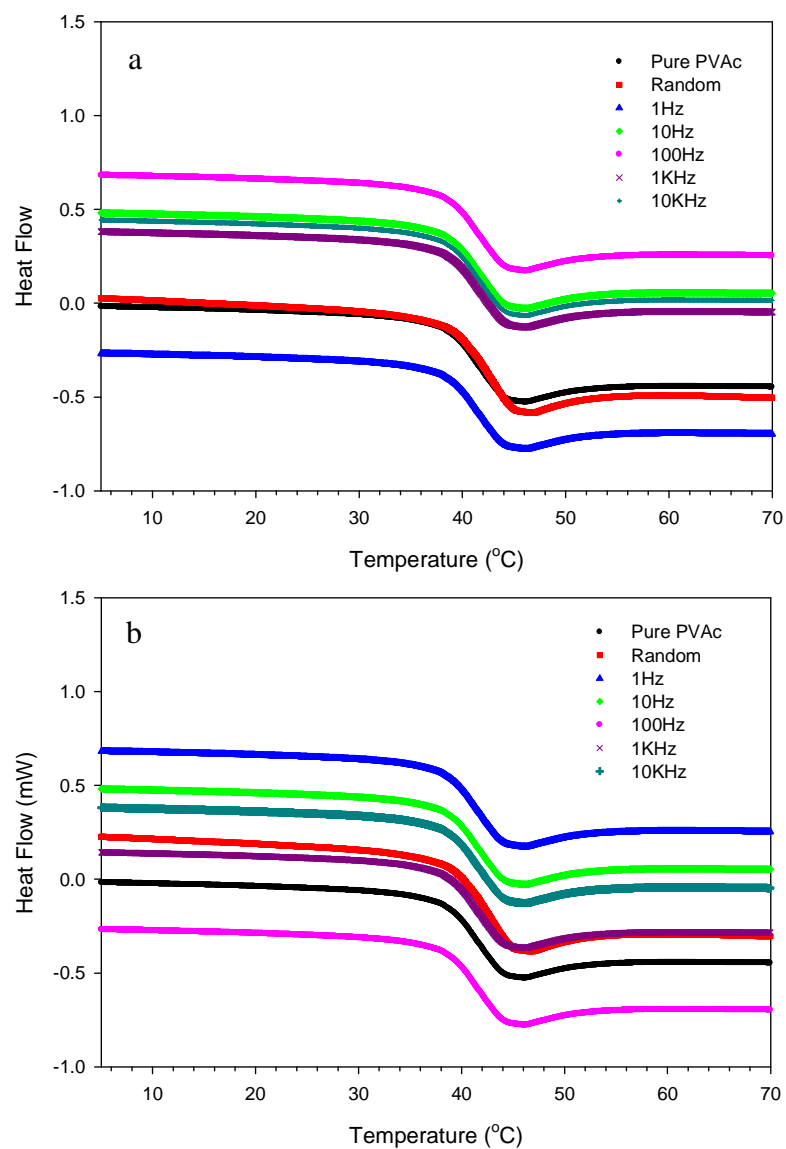


Figure 3.16: DSC curves of aligned sample (a) 100 V/mm and (b) 250 V/mm.

Table 3.2: T_g of aligned nanocomposites at $100V_{pp}/mm$ and $250V_{pp}/mm$

	T_g (100 V/mm)	T_g (250 V/mm)
Pure PVAc	$42.10^{\circ}\text{C} \pm 0.76$	$42.03^{\circ}\text{C} \pm 0.16$
Random	$42.14^{\circ}\text{C} \pm 0.34$	$42.01^{\circ}\text{C} \pm 0.52$
1 Hz	$42.21^{\circ}\text{C} \pm 0.45$	$42.12^{\circ}\text{C} \pm 0.22$
10 Hz	$41.94^{\circ}\text{C} \pm 0.12$	$41.04^{\circ}\text{C} \pm 1.2$
100 Hz	$42.03^{\circ}\text{C} \pm 0.95$	$42.00^{\circ}\text{C} \pm 0.1$
1 KHz	$42.24^{\circ}\text{C} \pm 1.03$	$42.07^{\circ}\text{C} \pm 0.42$
10 KHz	$42.28^{\circ}\text{C} \pm 0.25$	$42.18^{\circ}\text{C} \pm 0.11$

3.3.2 Water Absorption Study

Weight change experiments were carried out to see if the nanocomposites absorb water from the atmosphere. Table 3.3 below shows the weight change before and after tensile testing. It was found that the weight of the samples does not change before and after tensile testing leading us to believe that the nanocomposites do not absorb any moisture from the atmosphere.

Table 3.3: Weight change of pure PVAc and CWs nanocomposites before and after tensile testing

SAMPLE	Wt (g) (Before Testing)	Wt (g) (After Testing)
Pure	6.419 ± 0.14	6.419 ± 0.13
Random	6.325 ± 0.33	6.324 ± 0.33
1Hz	6.248 ± 0.01	6.248 ± 0.03
10 Hz	6.353 ± 0.6	6.354 ± 0.5
100 Hz	6.125 ± 0.22	6.124 ± 0.09
1KHz	6.632 ± 0.27	6.632 ± 0.3
10 KHz	6.269 ± 0.15	6.266 ± 0.06

3.3.3 Thermogravimetric Analysis

TGA was performed on pure PVAc and CWs/PVAc nanocomposites to quantitatively study water absorption of PVAc and CWs nanocomposites. The TGA curves of pure PVAc and CWs/PVAc composites are shown in Figure 3.17. The curves show that pure PVAc and CWs/PVAc composites do not absorb any water. This is evidenced by the absence of weight loss at 100°C.

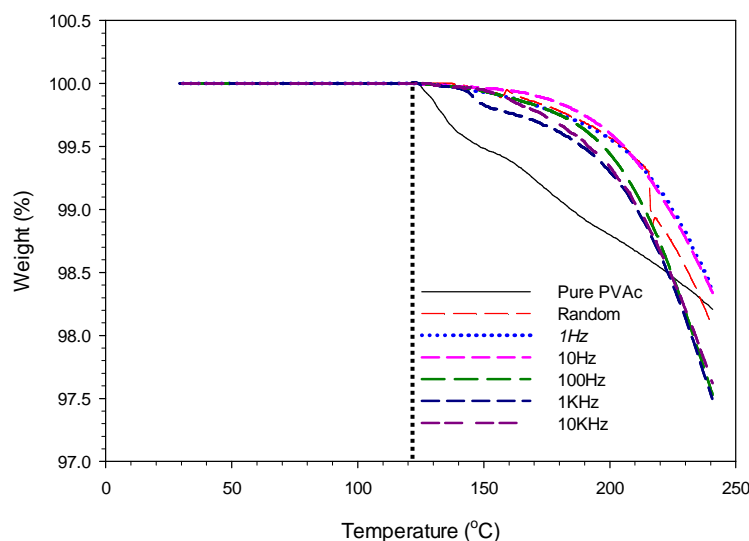


Figure 3.17: TGA of pure PVAc and CWs/PVAc nanocomposites.

3.3.4 Dynamic Mechanical Analysis

Dynamic mechanical measurements were done for pure PVAc and CWs reinforced nanocomposites parallel (L) and perpendicular (T) to the alignment direction. Storage modulus (E') as a function of temperature for samples parallel and perpendicular to the alignment direction show enhancement of E' for the aligned cases as compared to the pure PVAc and random case. Figure 3.18 shows storage modulus (parallel to alignment direction) as a function of temperature for the 250V/mm alignment case. At room temperature and above glass transition, the storage modulus was noisy. The DMA recommended sample lengths and widths are 30mm and 5mm respectively. After the alignment process the maximum sample length we could achieve was 18mm. Above the t_g , when there is long range molecular motion, the material

softens. Softening of the material makes it difficult to grip. Also, the length of the material we processed is much smaller than recommended. The reduced length in addition to softening of the material leads to slipping of the sample from the grips causing noise in the data.

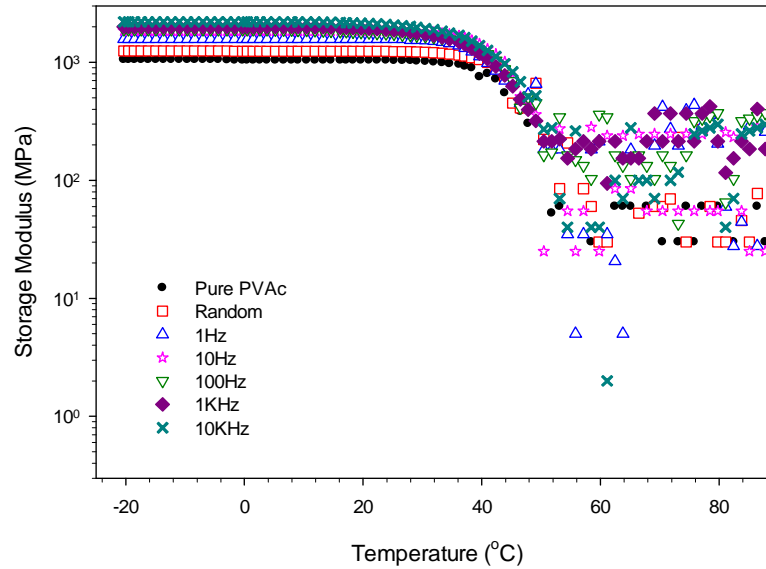


Figure 3.18: Storage modulus (parallel to alignment) as a function of temperature for 250V/mm case.

Figure 3.19 shows the storage modulus as a function of temperature for the 250V/mm case below the T_g . Below T_g (42°C), the storage modulus of pure PVAc and random were found to be 1 and 1.25 GPa respectively. For the alignment frequencies of 1Hz, 10Hz, 100Hz, 1KHz and 10KHz the storage moduli were found to be 1.54, 1.75, 1.90, 2.01 and 2.2 GPa respectively as listed in Table 3.4

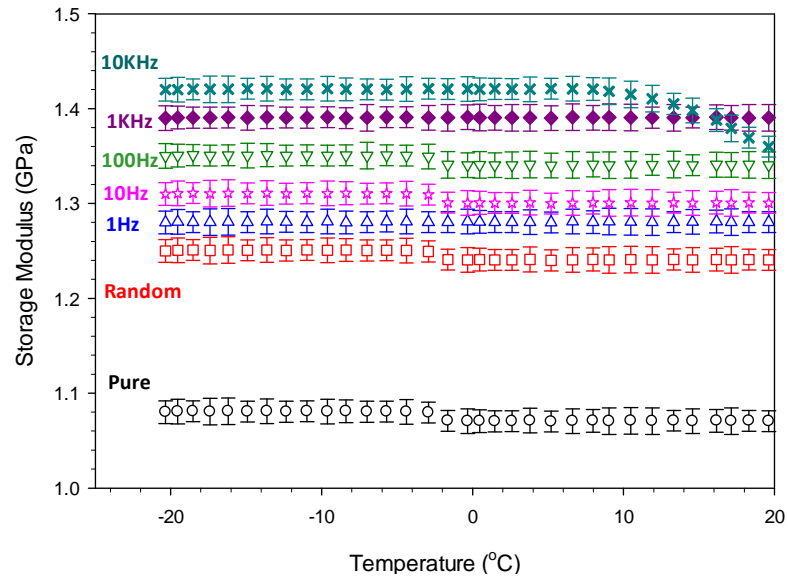


Figure 3.19: Storage modulus (parallel to alignment) as a function of temperature (below T_g) for 250V/mm case.

Table 3.4: Storage modulus (parallel to alignment) of pure PVAc, random and aligned cases below T_g and comparison of percentage increase in E'

Sample	E' (Gpa)	% Increase in E'	% Increase in E'
Pure	1.08 ± 0.012	-	-
Random	1.25 ± 0.014	15.74	-
1 Hz	1.54 ± 0.016	42.59	23.02
10 Hz	1.75 ± 0.016	62.03	40.00
100 Hz	1.90 ± 0.020	75.93	51.99
1 KHz	2.01 ± 0.025	86.11	60.79
10 KHz	2.22 ± 0.027	105.56	77.60

Figure 3.20 shows storage modulus (perpendicular to alignment) as a function of temperature for the 250V/mm alignment case. As in the case of composites parallel to the direction of alignment, increase in E' was observed for samples perpendicular to the alignment direction.

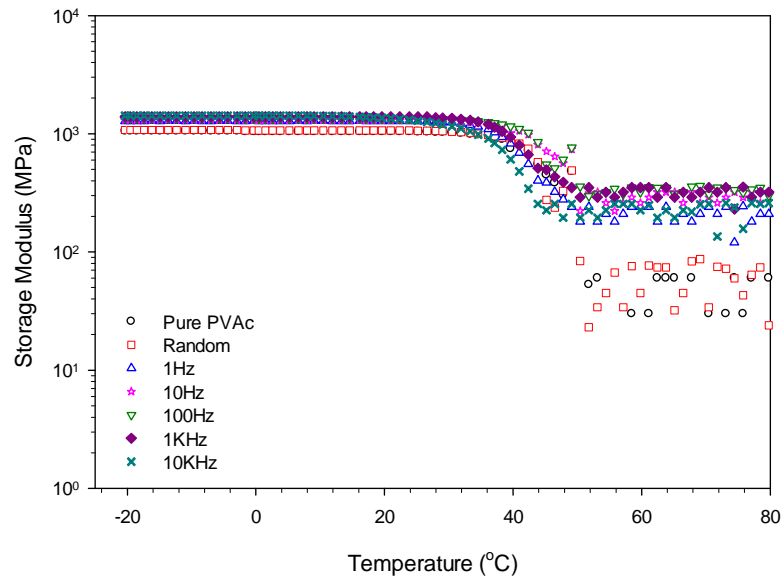


Figure 3.20: Storage modulus (perpendicular to alignment) as a function of temperature for 250V/mm case.

Figure 3.21 shows the storage modulus as a function of temperature for the 250V/mm case below the T_g . Below T_g (42°C), the storage modulus of pure PVAc and random were found to be 1 and 1.25 GPa respectively. For the alignment frequencies of 1Hz, 10Hz, 100Hz, 1KHz and 10KHz the storage moduli were found to be 1.28, 1.31, 1.35, 1.39 and 1.42 GPa respectively.

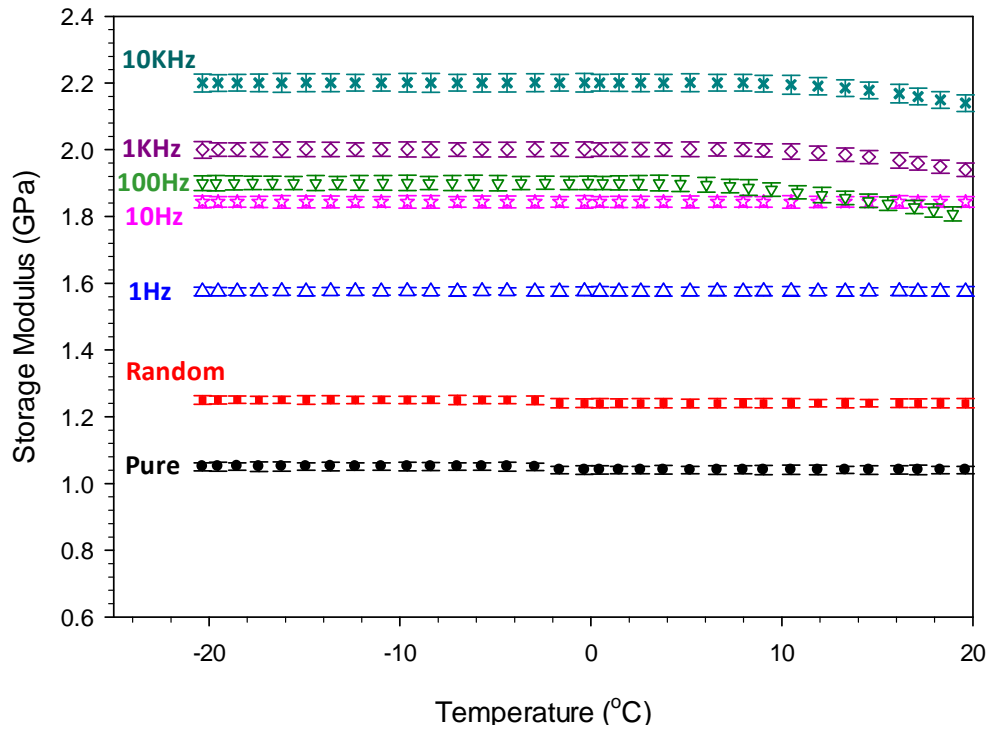


Figure 3.21: Storage modulus (perpendicular to alignment) as a function of temperature (below T_g) for 250V/mm case.

Table 3.5: Storage modulus (perpendicular to alignment) of pure PVAc, random and aligned cases below T_g and comparison of percentage increase in E'

Sample	E' (Gpa)	% Increase in E'	% Increase in E'
Pure	1.08 ± 0.01	-	-
Random	1.25 ± 0.013	15.74	-
1 Hz	1.28 ± 0.011	18.52	2.40
10 Hz	1.31 ± 0.009	21.29	4.80
100 Hz	1.35 ± 0.021	25.00	8.00
1 KHz	1.39 ± 0.024	28.70	11.19
10 KHz	1.42 ± 0.029	31.38	13.59

A 77% and 13% increase in storage modulus below the T_g (parallel and perpendicular to alignment direction respectively) was observed as a function of alignment frequency for the optimal alignment parameters (250V_{pp}/mm and 10KHz for a duration of 1 hour) as compared to pure PVAc. This kind of reinforcement below the T_g is usually not seen in polymer nanocomposites. As the alignment frequency is increased, the CWs come close to each other and form chains. When left over time the chains start interacting with each other forming thicker chains as seen in Figure 3.12. When the CWs chains come close to each other, they start interacting with each other due to the strong hydrogen bond forming affinity between the OH⁻ groups of the CWs leading to formation of 3D networks. Therefore, the significant reinforcement observed for the aligned cases (parallel to alignment) is possibly due to chain formation, thickening of chains and possible hydrogen bonding between the CWs chains. As for the samples tested perpendicular to alignment direction the hydrogen bonding seems to be contributing to the enhancement in modulus.

3.3.4.1 Theoretical Predictions

Modeling of the mechanical properties based on rule of mixtures and Halpin-Tsai equations were carried out to determine the theoretical predictions. Halpin-Tsai equations are normally used to predict the modulus of random and unidirectional short fiber composites (SF) [66]. Rule of mixtures is used to predict the modulus of continuous long fiber composites (LF) [67]. The following data was used in the

calculations: $E_{CW}=145$ GPa, $E_{PVAc}= 1.08$ GPa, Aspect ratio=32 and Volume fraction = 0.00315 (weight fraction = 0.004). The values of elastic modulus of the CWs (E_{CW}) and PVAc (E_{PVAc}) were taken from the literature. The aspect ratio of 32 was calculated by averaging the lengths and diameters of 150 individually dispersed CWs from the SEM and AFM pictures shown in section 3.1.3. A weight percent of 0.4 was used for this study. The volume fraction was calculated by converting wt% to vol% and dividing it by 100. To account for randomness of short fibers a parameter ‘ α ’ was introduced [66]. If fiber length is smaller than thickness of specimen, fibers are assumed to be randomly oriented in 3D and $\alpha = 1/6$. The Halpin-Tsai equation for randomly aligned short fiber composites (MH) is as follows:

$$E_c = \frac{1 + 2\left(\frac{l}{d}\right)\eta_f V_f}{1 - \eta_f V_f} E_m \quad (3)$$

$$\eta_f = \frac{\frac{\alpha E_f}{E_m} - 1}{\frac{\alpha E_f}{E_m} + 2\left(\frac{l}{d}\right)} \quad (4)$$

Where,

E_c, E_f, E_m = Elastic modulus of composite, CWs and PVAc respectively

α = Randomness factor (1/3)

l/d = Aspect ratio of CWs

V_f = Volume fraction of CWs

A comparison of the experimental and theoretical results for the random case using equations (1) and (2) are presented in Figure 3.22. The experimental results for random were in very good correlation with the Halpin-Tsai theoretical results.

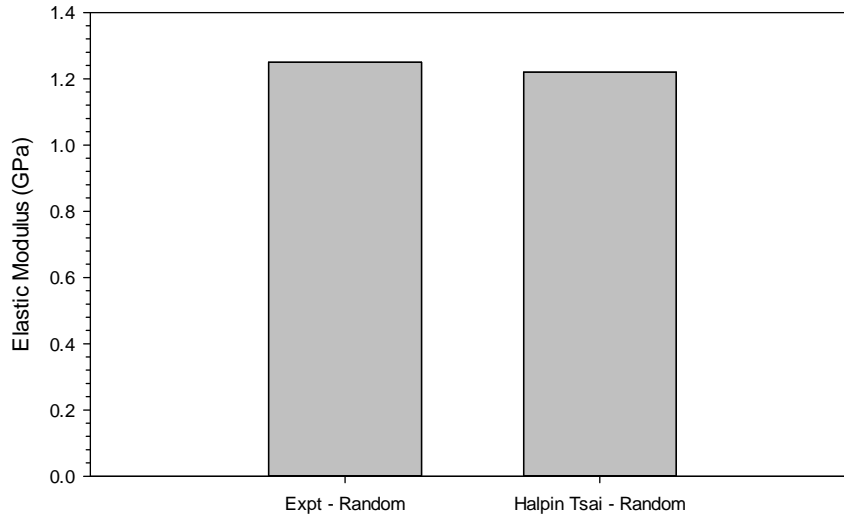


Figure 3.22: Experimentally measured modulus compared to theoretical predictions by Halpin-Tsai for randomly oriented composites.

Theoretical predictions for unidirectional short and continuous long fiber composites were also carried out. For aligned long fiber composites, the longitudinal stiffness (LF-L) is expressed as:

$$E_{C,L} = E_f V_f + E_m (1 - V_f) \quad (5)$$

and the transverse stiffness (LF-T) is expressed as:

$$\frac{1}{E_{C,T}} = \frac{V_f}{E_f} + \frac{V_m}{E_m} \quad (6)$$

For unidirectional short fiber composites, the longitudinal stiffness (SF-L) is expressed as:

$$E_{c,L} = \frac{1 + 2\left(\frac{l}{d}\right)\eta_f V_f}{1 - \eta_f V_f} E_m \quad (7)$$

Where,

$$\eta_f = \frac{E_f - E_m}{E_f + 2\left(\frac{l}{d}\right)E_m} E_m \quad (8)$$

The transverse stiffness (SF-T) is expressed as:

$$E_{c,T} = \frac{1 + 2\eta_f V_f}{1 - \eta_f V_f} E_m \quad (9)$$

Where,

$$\eta_f = \frac{E_f - E_m}{E_f + 2E_m} E_m \quad (10)$$

$E_{c,L}$ and $E_{c,T}$ = Elastic modulus of composite in the longitudinal and transverse directions

E_f , E_m = Elastic modulus CWs and PVAc respectively

V_f = Volume fraction of CWs

Figure 3.23 shows the comparison of experimental results (random and samples parallel to the alignment direction) to random, unidirectional short and continuous long fiber composites. Both unidirectional short and continuous long fibers composite models were used to account for possible alignment and chain formation of CWs in PVAc. As discussed before, the random results from experiments and Halpin-Tsai predictions

correlate well. However, the Halpin-Tsai equations and rule of mixtures for unidirectional short and continuous long fiber composites underestimate the longitudinal elastic modulus of the aligned CW nanocomposites.

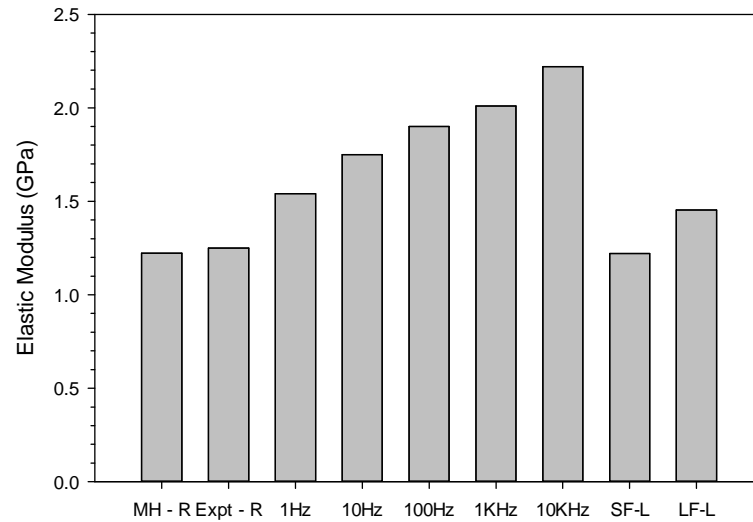


Figure 3.23: Comparison of experimental results (parallel to alignment) to rule of mixture and Halpin-Tsai predictions.

Figure 3.24 shows the comparison of experimental results (random and samples perpendicular to the alignment direction) to predictions for random, transverse unidirectional short and continuous long fiber composites. Similar to the experimental results for samples parallel to the alignment direction, the Halpin-Tsai and rule of mixtures for unidirectional short and long fiber perpendicular to alignment direction seem to underestimate the elastic modulus of aligned CWs nanocomposites.

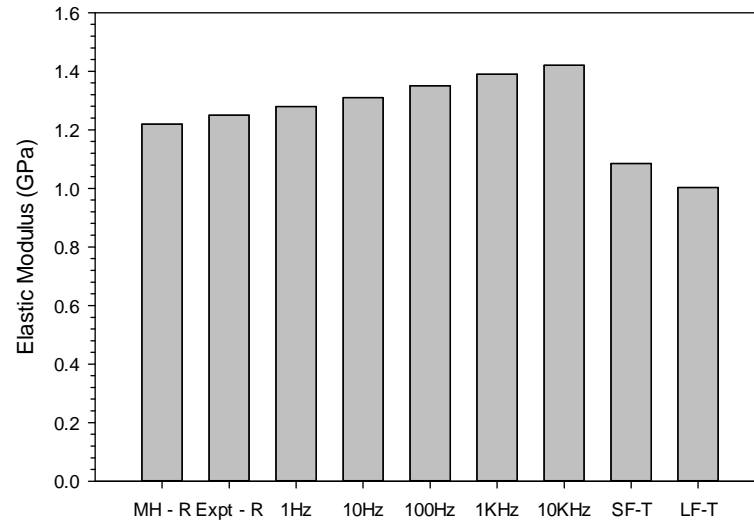


Figure 3.24: Comparison of experimental results (perpendicular to alignment) to rule of mixtures and Halpin-Tsai predictions.

This underestimation could be because the Halpin-Tsai and rule of mixtures assume that there is no interaction between fibers. However, in our case we do expect interaction between CWs and CWs chains. The tendency of the CWs to form hydrogen bonds seems to be contributing to the reinforcement. Figure 3.25 shows a comparison of experimental results (parallel and perpendicular to alignment direction) to Halpin-Tsai predictions for unidirectional short and continuous long fiber composites.

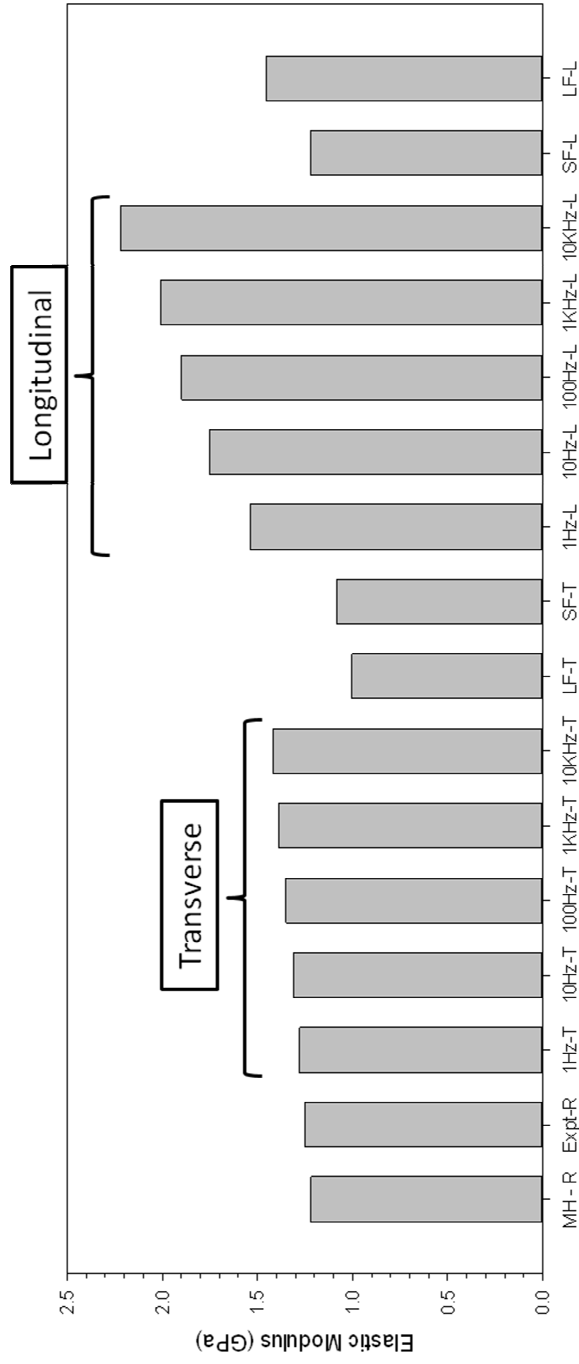


Figure 3.25: Comparison of experimental results (parallel and perpendicular to alignment direction) to rule of mixtures and Halpin-Tsai predictions.

3.3.5 Static Tensile Testing

Since the data from the DMA at room temperature and above glass transition was noisy, static tensile testing was performed to measure the mechanical properties. Tensile tests were performed to obtain mechanical properties at room temperature and above T_g (50 °C). Figure 3.26 shows the stress-strain curves for pure PVAc, random and aligned cases (parallel to alignment direction) at room temperature. Figure 3.27 shows the initial portion of the stress strain curve. The elastic modulus of pure PVAc was found to be 35 MPa. The elastic modulus increases to 66.52 MPa with the addition of 0.4wt% CWs. The elastic modulus at 1Hz alignment frequency was found to be 102.26 MPa. As the alignment frequency is increased for 1 Hz to 10 KHz the elastic modulus increases.

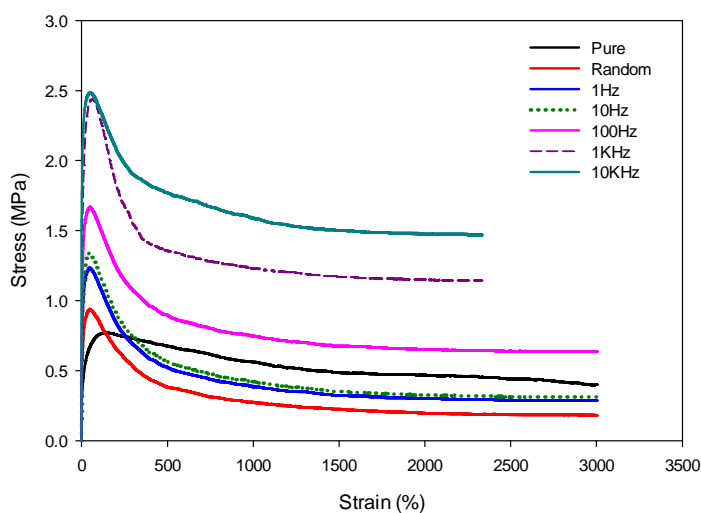


Figure 3.26: Stress vs strain curves for pure PVAc, random and aligned cases (parallel to alignment direction) at room temperature.

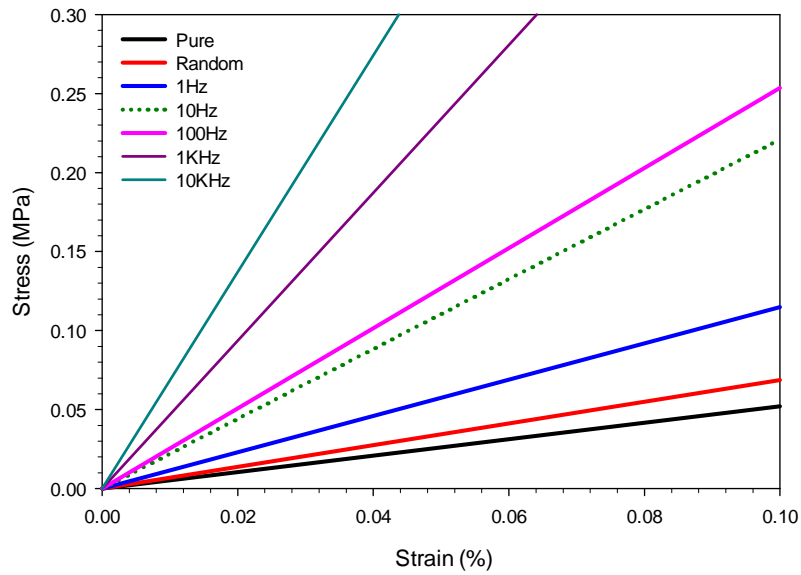


Figure 3.27: Initial portion of the stress vs strain curves for pure PVAc, random and aligned cases (parallel to alignment direction) at room temperature.

The highest increase in elastic modulus was obtained for the 10 KHz alignment frequency case. Table 3.6 shows the elastic modulus of the pure PVAc, random and aligned cases and comparison of percentage increase in elastic modulus. An 88, 191, 257, 278, 305 and 325% increase in elastic modulus was achieved for random, 1Hz, 10Hz, 100Hz, 1 KHz and 10KHz cases respectively as compared to pure PVAc. A 54, 89, 100, 115 and 125% increase in elastic modulus was achieved for 1Hz, 10 Hz, 100Hz, 1 KHz and 100 KHz cases respectively as compared to the random case.

Table 3.6: Elastic modulus of pure PVAc, random and aligned cases at room temperature and comparison of percentage increase in elastic modulus

Sample	Modulus (MPa)	% Increase in E	% Increase in E
Pure PVAc	35 ± 1.3		-
Random	66.52 ± 0.9	-	88
1Hz	102.26 ± 1.1	54	191
10Hz	125.14 ± 0.4	89	257
100Hz	132.58 ± 0.31	100	278
1KHz	142.23 ± 0.54	115	305
10 KHz	149.42 ± 0.76	125	325

The tensile strength for pure PVAc was found to be 0.5 MPa. With the addition of 0.4wt% CWs the tensile strength increases to 0.95 MPa. After the application of electric field, the tensile strength increase as a function of alignment frequency. The tensile strength at 1Hz, 10Hz, 100Hz, 1 KHz and 10 KHz alignment frequencies were found to be 1.2, 1.5, 1.7, 2.3 and 2.5 MPa respectively as shown in Table 3.7. The percent elongation for pure PVAc, random, 1Hz, 10 Hz and 100Hz was ~3000. At 1 and 10 KHz the elongation at break drops to 2400. A 20% reduction in elongation was observed

Table 3.7: Tensile strength and elongation at break for pure PVAc, random and aligned cases at room temperature

Sample	Tensile Strength (Mpa)	% Elongation
Pure PVAc	0.52 ± 0.10	3002 ± 96
Random	0.95 ± 0.22	2996 ± 112
1Hz	1.21 ± 0.13	2999 ± 56
10 Hz	1.53 ± 0.09	3003 ± 43
100 Hz	1.71 ± 0.12	3002 ± 12
1KHz	2.34 ± 0.31	2380 ± 44
10 KHz	2.53 ± 0.15	2368 ± 81

Figure 3.28 shows the stress vs strain curve for pure PVAc, random and aligned cases (parallel to alignment direction) at 50°C. Figure 3.29 shows the initial portion of the stress-strain curve. The elastic modulus of Pure PVAc was found to be 0.29 MPa. The elastic modulus increases to 1.18 MPa with the addition of 0.4wt% CWs. The elastic modulus at 1Hz alignment frequency was found to be 1.22 MPa. As the alignment frequency is increased for 1 Hz to 10 KHz the elastic modulus increases. The highest increase in elastic modulus was obtained for the 10 KHz alignment frequency case.

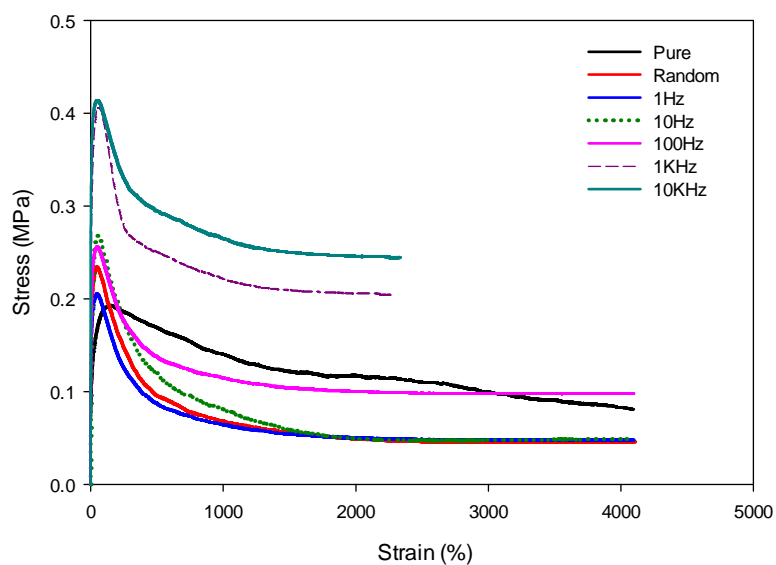


Figure 3.28: Stress vs strain curves for pure PVAc, random and aligned cases (parallel to alignment direction) at 50°C.

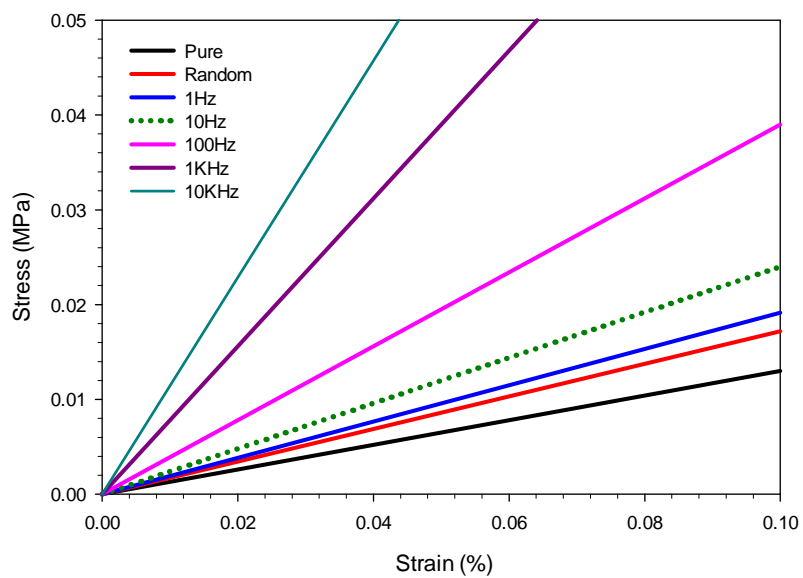


Figure 3.29: Initial portion of the Stress vs strain curves for pure PVAc, random and aligned cases (parallel to alignment direction) at 50°C.

Table 3.8 shows elastic modulus of pure PVAc, random and aligned cases and comparison of percentage increase in elastic modulus. A 306, 320, 427, 479, 583 and 680% increase in elastic modulus was achieved for random, 1Hz, 10Hz, 100Hz, 1 KHz and 10 KHz cases respectively as compared to pure PVAc. A 4, 30, 43, 68 and 91% increase in elastic modulus was achieved for 1Hz, 10 Hz, 100Hz, 1 KHz and 10 KHz cases respectively as compared to the random case. The tensile strength for pure PVAc was found to be 0.14 MPa. With the addition of 0.4wt% CWs the tensile strength increases to 0.18 MPa. After the application of electric field, the tensile strength increase as a function of alignment frequency.

Table 3.8: Elastic modulus of pure PVAc, random and aligned cases at 50°C and comparison of percentage increase in elastic modulus

Sample	Elastic Modulus (Mpa)	% Increase In E	% Increase In E
Pure PVAc	0.29 ± 0.1	-	-
Random	1.18 ± 0.05	0	306.89
1Hz	1.22 ± 0.04	3.38	320.68
10 Hz	1.53 ± 0.17	29.66	427.58
100 Hz	1.68 ± 0.12	43.22	479.31
1KHz	1.98 ± 0.12	67.79	582.75
10 KHz	2.26 ± 0.25	91.52	679.31

The tensile strength at 1Hz, 10Hz, 100Hz, 1 KHz and 10 KHz alignment frequencies were found to be 0.16, 0.25, 0.24, 0.41 and 0.43 MPa respectively as shown in Table 3.9. The percent elongation for pure PVAc, random, 1Hz, 10 Hz and 100Hz was ~4000%. At 1 and 10 KHz the elongation at break drops to 2700%. A 32 percent decrease in percent elongation was observed.

Table 3.9: Tensile strength and elongation at break for pure PVAc, random and aligned cases at 50°C

Sample	Tensile Strength (Mpa)	% Elongation
Pure PVAc	0.14 ± 0.05	4087 ± 42
Random	0.18 ± 0.12	4082 ± 19
1Hz	0.23 ± 0.09	4005 ± 31
10 Hz	0.26 ± 0.10	4012 ± 76
100 Hz	0.27 ± 0.04	4019 ± 9
1KHz	0.41 ± 0.06	2678 ± 52
10 KHz	0.44 ± 0.02	2662 ± 13

Tensile tests were performed on pure PVAc, random and aligned composites (perpendicular direction of alignment) at 50°C. Figure 3.30 shows the stress vs. strain curve for pure PVAc, random and aligned cases. The elastic modulus of Pure PVAc was found to be 0.29 MPa. The elastic modulus increases to 1.18 MPa with the addition of 0.4wt% CWs. Figure 3.31 shows the Initial portion of the stress vs strain curves (perpendicular to alignment direction) at 50°C. The elastic modulus at 1Hz alignment frequency was found to be 1.20 MPa. As the alignment frequency is increased for 1 Hz to 10 KHz the elastic modulus increases to 1.34 MPa.

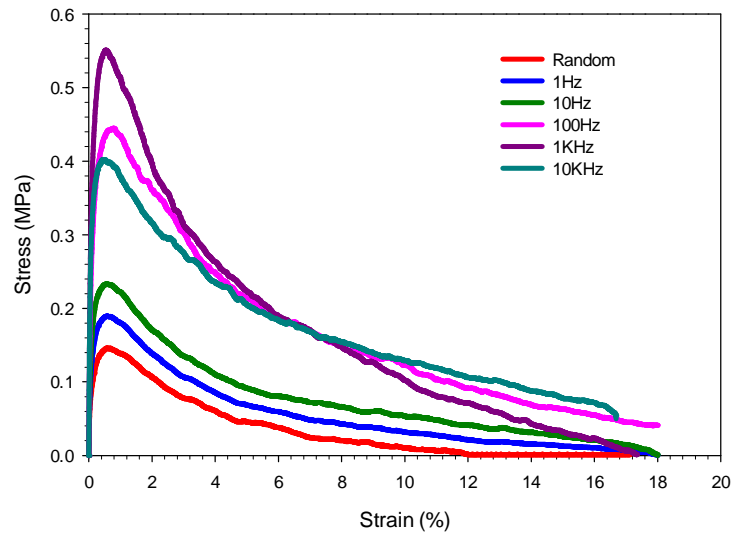


Figure 3.30: Stress vs strain curves for pure PVAc, random and aligned cases (perpendicular to alignment direction) at 50°C.

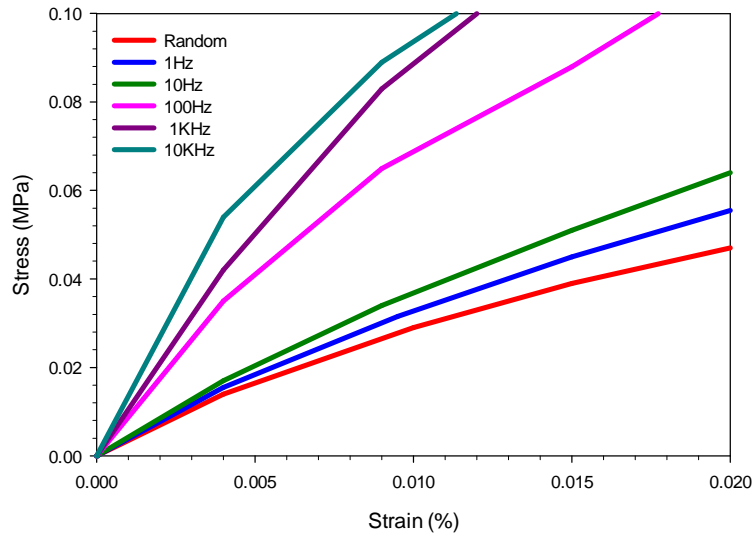


Figure 3.31: Initial portion of the stress vs strain curves (perpendicular to alignment direction) at 50°C.

The highest increase in elastic modulus was obtained for the 10 KHz alignment frequency case. A 306, 313, 324, 337, 348 and 362% increase in elastic modulus was achieved for random, 1Hz, 10Hz, 100Hz, 1 KHz and 10 KHz cases as compared to pure PVAc and a 1.5, 4, 7.5, 10 and 13% increase in elastic modulus was achieved for 1Hz, 10 Hz, 100Hz, 1 KHz and 10 KHz cases as compared to random case as shown in Table 3.6. The tensile strength at 1Hz, 10Hz, 100Hz, 1 KHz and 10 KHz alignment frequencies were found to be 1.18, 1.20, 1.23, 1.27, 1.30 and 1.34 MPa respectively as shown in Table 3.10. The percent elongation for pure PVAc, random, 1Hz, 10 Hz and 100Hz was ~1930%. There was no reduction in % elongation for aligned cases.

Table 3.10: Elastic modulus of pure PVAc, random and aligned cases (perpendicular to alignment) at room temperature and comparison of percentage increase in elastic modulus

Sample	Elastic Modulus (MPa)	% Increase In E	% Increase In E
Pure PVAc	0.29 ± 0.10	-	-
Random	1.18 ± 0.30	-	306.89
1Hz	1.20 ± 0.08	1.69	313.79
10 Hz	1.23 ± 0.03	4.24	324.14
100 Hz	1.27 ± 0.04	7.62	337.93
1KHz	1.30 ± 0.20	10.17	348.27
10 KHz	1.34 ± 0.14	13.56	362.07

Table 3.11: Tensile strength and elongation at break for pure PVAc, random and aligned cases (perpendicular to alignment) at room temperature

Sample	Tensile Strength (Mpa)	%Elongation
Pure PVAc	0.1 ± 0.05	1932 ± 12
Random	0.14 ± 0.12	1963 ± 16
1Hz	0.19 ± 0.07	1943 ± 4
10 Hz	0.24 ± 0.04	1939 ± 6
100 Hz	0.42 ± 0.06	1965 ± 13
1KHz	0.54 ± 0.1	1935 ± 7
10 KHz	0.45 ± 0.14	1942 ± 11

Table 3.12 shows a comparison modulus enhancement we achieved with previous findings. In CWs/latex systems, Favier et al achieved 156% increase in modulus at 1wt% loading, Helbert et al achieved 500% increase in modulus at 5 wt% CWs loading. In other CWs systems, Samir et al achieved 4% increase in modulus at 3 wt% POE and Li et al achieved 227% increase with 1 wt% in POE and PU respectively. In CWs/PVAc systems, Capadona and Shanmuganathan et al achieved 360 and 566% increase in modulus at 1 and 4wt% respectively. As indicated in Table 3.8 , a 680%

increase (this study) in modulus at 0.4 wt% CWs. This demonstrates the advantage of aligning CWs to achieve significant improvements in mechanical properties at low weight content. This is a drastic improvement compared to other findings in the literature.

Table 3.12: Comparison of modulus enhancement we achieved with previous findings

Material System	Studies	Concentration (wt%)	Improvement in E (%)
CWs + PVAc	This Study	0.4	680
CWs + Latex	Favier [20]	1	156
CWs + Latex	Helbert [33]	5	500
CWs + POE	Samir [68]	3	4
CWs + PU	Li	1	227
CWs + PVAc	Shanmuganathan [47]	4	566
CWs + PVAc	Capadona [46]	1	360

4. CONCLUSIONS

The main objective of this work was to improve the mechanical and dielectric properties of cellulose based polymer nanocomposites by using low concentrations of CWs so as not to detrimentally affect toughness and ductility. To accomplish this objective, an AC electric field was used to align low concentrations of uniformly dispersed CWs in PVAc.

Firstly, we focused on developing a processing method to achieve homogeneous dispersion of CWs. Two different dispersion methods were used - basic and modified method. The basic method was based on magnetic stirring and bath sonication. Homogeneous dispersion of CWs was achieved by increasing the sonication time. The sonication process breaks down the large CWs agglomeration and helps in preventing re-agglomeration of CWs. OMs of the basic method showed CWs were dispersed as small bundles ($< 50\mu\text{m}$) and not as individual whiskers, resulting in a microcomposite. Following results from DSC which pointed to the possibility of water (present in as-received CWs) acting as a plasticizer, a modified dispersion method was developed. A solvent transfer process was used wherein the water present in CWs was removed by centrifuging the CWs in DMF. Repeated washes with DMF led to complete removal of water, as verified by TGA. A high power sonication method was used to exfoliate the CWs. The optimal parameters of sonication were found to be 450 W power for duration of 70 minutes. For the optimal parameters, CWs were individually dispersed with average lengths and diameters of $\sim 260\text{ nm}$ and $\sim 8\text{ nm}$ respectively yielding an aspect

ratio of approximately 32. The dimensions of the as received CWs in water were ~260nm in length and ~6nm in diameter. Comparing the dimensions of the dispersed CWs by the modified method to those of the as-received CWs dispersed in water, we conclude that the modified dispersion method does lead to individually dispersed whiskers in DMF and PVAc.

Secondly, we focused on developing a methodology that is amenable to composite processing with aligned cellulose to study the effect of AC electric field on the behavior of CWs in silicone oil and polymer composites.

In the case of silicone oil, the effect of AC electric field was evaluated as a function of electric field magnitude, frequency and duration of applied electric field. The CWs response to the applied electric field was a two step process: Firstly, the CWs rotated in the direction of the electric field. Secondly, the ends of the CWs interacted with each other and formed long chains in the direction of the electric field. Finally the chains interacted with each other to form thicker chains. The driving force for chain formation is believed to be dielectrophoresis. The degree of alignment of CWs in silicone oil was dependent on the alignment frequency, electric field magnitude and time. The optimal parameters of alignment for the CWs in silicone oil were found to be $3000V_{pp}/mm$ and 500 mHz for a duration of 20mins.

In the case of PVAc, the behavior of CWs under an applied electric field was similar to that of the silicone oil study. The degree of alignment of CWs in PVAc was dependent on the alignment frequency, electric field magnitude and time. The optimal parameters of alignment for the CWs in PVAc using the basic method were found to be

200V_{pp}/mm and 50 KHz for duration of 20mins and 250V/mm, The optimal parameters of alignment for the CWs in PVAc using the modified method were found to be 250V_{pp}/mm and 10KHz for a duration of 60 minutes respectively. In-situ dielectric measurements of all the three solutions (CWs/Silicone oil, micro CWs/PVAc and nano CWs/PVAc) were done to gauge the extent of alignment. Increase in dielectric constant was achieved as a function of alignment parameters. The highest increase (133%) in dielectric constant for CWs aligned in silicone oil was achieved at 300V_{pp}/mm and 500 mHz for a duration of 20 minutes. The highest increase (77% and 22%) in dielectric constant for micro CWs and nano CWs aligned in PVAc respectively.

Finally, we focused on exploring the impact on physical properties of aligned CWs reinforced polymer nanocomposites. Dielectric constant measurements were done on the aligned nanocomposites made by the modified method. After solvent evaporation the sample were dried further to remove any residual solvent. The samples were then electroded and dielectric constant measurements were done. An enhancement in dielectric constant as a function of alignment frequency was achieved. At 100V/mm, a slight increase in dielectric constant was achieved for the aligned cases as compared to random. However, there was no contrast in dielectric constant as a function of alignment frequency. At 250V/mm, improvement in dielectric constant as well as contrast between different alignment frequencies was achieved. Significant improvements in modulus as a function of alignment frequency were achieved below T_g (42°C, at room temperature and above T_g when the samples were tested along alignment direction. Below T_g , a 76% and 100% increase in storage modulus was achieved for 10 KHz alignment frequency

case as compared to random and pure PVAc. At room temperature and above T_g a 325% and 680% enhancement was achieved respectively as compared to pure PVAc. Significant improvements of 400% and 210% in tensile strength were achieved at room temperature and above the T_g respectively. A moderate 23% decrease in elongation at break was observed for the 10 KHz alignment case. Improvements in modulus as a function of alignment frequency were also achieved when the samples were tested perpendicular to the alignment direction. A 32% and 300% increase in modulus was achieved for the 10 KHz as compared to random and pure PVAc. Rule of mixtures and Halpin-Tsai equations were used to compare to the experimental results. The experimental results for random correlated well with the random Halpin-Tsai predictions. However, the theoretical models underestimate the modulus of the aligned composites. This is because the models do not take into consideration the interaction between the particles. The significant improvement in mechanical properties at 0.4wt% CWs in PVAc is attributed to the alignment, chain formation and strongly interconnected 3D network formed due to CWs interacting with each other.

Through a variety of characterization techniques, we showed that significant improvements in physical properties can be achieved by electric field manipulation of CWs polymer nanocomposites. Electric field magnitude, frequency and duration of electric field can be varied to achieve desired physical properties at very low CWs loadings by not detrimentally affecting toughness and ductility.

4.1 Recommendations for Future Work:

- 1) In terms of the aligned microstructure, the next step should focus on probing the microstructure of aligned CWs.
 - a) Develop a sample preparation method (possibly dyeing the CWs before alignment or argon gas etching to remove polymer layer) to probe the microstructure possibly using TEM and AFM
- 2) Exploring the possibility of using CWs for sensing and actuation applications.
 - a) Cellulose is known to be an electroactive polymer. Reinforce polymers like polyvinylidene fluoride (PVDF) and polyamides with aligned CWs and characterize composites for possible electromechanical coupling.

REFERENCES

- [1] M. A. S. Azizi Samir, F. Alloin and A. Dufresne, "Review of recent research into cellulosic whiskers, their properties and their application in nanocomposite field," *Biomacromolecules*, vol. 6, pp. 612-626, 2005.
- [2] S. Eichhorn, A. Dufresne, M. Aranguren, N. Marcovich, J. Capadona, *et al.*, "Review: Current international research into cellulose nanofibres and nanocomposites," *J. Mat. Sci.*, vol. 45, pp. 1-33, 2010.
- [3] S. Hill, "Cars that grow on trees. New Scientist," pp. 36-39, 1997.
- [4] Kozłowski R and M. B, "New trends in the utilization of by products of fibre crops residue in pulp and paper industry, building engineering, automotive industry and interior furnishing. ," in *Proc. Int. Symp. Nat. Poly. Comp, San Paulo*, pp. 504-510, 2000.
- [5] B. Dahlke, H. Larbig, H. D. Scherzer and R. Poltrock, "Natural fiber reinforced foams based on renewable resources for automotive interior applications," *J. Cell. Plast.*, vol. 34, pp. 361-379, July 1, 1998 1998.
- [6] A. S. Herrmann, J. Nickel and U. Riedel, "Construction materials based upon biologically renewable resources—from components to finished parts," *Polym. Degrad. Stab.*, vol. 59, pp. 251-261, 1998.
- [7] Bazhenov VA, "Piezoelectric properties of woods," in *Consultants bureau*, ed. New York, 1961.
- [8] E. Fukada, "History and recent progress in piezoelectric polymers," *Ultrasonics, Ferroelectrics and Frequency Control, IEEE Transactions*, vol. 47, pp. 1277-1290, 2000.
- [9] J. Kim, S. Yun and Z. Ounaies, "Discovery of cellulose as a smart material," *Macromolecules*, vol. 39, pp. 4202-4206, 2006.
- [10] J. Kim, "Electroactive-paper actuator made with cellulose/NaOH/urea and sodium alginate," *Cellulose*, vol. 14, pp. 217-223, 2007.

- [11] W. Niangui and Wang, "Electro-active paper made with aqueous cellulose solution," in *Proc SPIE-Int Soc Opt Eng.*, pp. 61680L-1, 2006.
- [12] J. Kim, "Role of inherent polarization and ion transport in the actuation of cellulose-based EAPap," in *Proc SPIE-Int Soc Opt Eng.*, vol. 5761, pp. 81-89, 2005.
- [13] H. S. Kim, Y. Li and J. Kim, "Electro-mechanical behavior and direct piezoelectricity of cellulose electro-active paper," *Sens. Actuators, A*, vol. 147, pp. 304-309, 2008.
- [14] H. Kim, "Characterization of piezoelectric effect and mechanical properties of cellulose based electro-active paper actuator," in *Proc SPIE-Int Soc Opt Eng.*, vol. 6170, p. 61701N, 2006.
- [15] S. Heung, "Piezoelectric effect of electro-active paper materials," *Key Eng. Mater.*, vol. 236, pp. 1507-10, 2006.
- [16] Z. Cai, C. Hou and G. Yang, "Characteristics and bending performance of electroactive polymer blend made with cellulose and poly(3-hydroxybutyrate)," *Carbohydr. Polym.*, vol. 87, pp. 650-657, 2012
- [17] A. Dufresne, M. B. Kellerhals and B. Witholt, "Transcrystallization in Mcl-PHAs/cellulose whiskers composites," *Macromolecules*, vol. 32, pp. 7396-7401, 1999.
- [18] P. Terech, L. Chazeau and J. Y. Cavaille, "A small-angle scattering study of cellulose whiskers in aqueous suspensions," *Macromolecules*, vol. 32, pp. 1872-1875, 1999.
- [19] I. Kvien and K. Oksman, "Orientation of cellulose nanowhiskers in polyvinyl alcohol," *Appl. Phys. A-Mater.*, vol. 87, pp. 641-643, 2007.
- [20] V. Favier, H. Chanzy and J. Y. Cavaille, "Polymer nanocomposites reinforced by cellulose whiskers," *Macromolecules*, vol. 28, pp. 6365-6367, 1995.

- [21] M. Grunert and W. T. Winter, "Nanocomposites of cellulose acetate butyrate reinforced with cellulose nanocrystals," *J. Polym. Environ.*, vol. 10, pp. 27-30, 2002.
- [22] X. M. Dong, J.-F. Revol and D. G. Gray, "Effect of microcrystallite preparation conditions on the formation of colloid crystals of cellulose," *Cellulose*, vol. 5, pp. 19-32, 1998.
- [23] S. Beck-Candanedo, M. Roman and D. G. Gray, "Effect of reaction conditions on the properties and behavior of wood cellulose nanocrystal suspensions," *Biomacromolecules*, vol. 6, pp. 1048-1054, 2005.
- [24] H. K. Chanzy, J. F., Phillips, G. O., Williams, P. A., *Cellulose Sources and Exploitation*: Eds.; Ellis Horwood Ltd.: New York, 1990.
- [25] M. Pääkkö, M. Ankerfors, H. Kosonen, A. Nykänen, S. Ahola, *et al.*, "Enzymatic hydrolysis combined with mechanical shearing and high-pressure homogenization for nanoscale cellulose fibrils and strong gels," *Biomacromolecules*, vol. 8, pp. 1934-1941, 2007.
- [26] R.J. Moon, *MacGraw-Hill Year Book of Science and Technology*. New York: McGraw Hill, 2008.
- [27] I. Kvien, B. S. Tanem and K. Oksman, "Characterization of cellulose whiskers and their nanocomposites by atomic force and electron microscopy," *Biomacromolecules*, vol. 6, pp. 3160-3165, 2005.
- [28] M. N. Anglès and A. Dufresne, "Plasticized starch/tunicin whiskers nanocomposites. 1. structural analysis," *Macromolecules*, vol. 33, pp. 8344-8353, 2000.
- [29] G. D. Fleming K, Matthews S, "A new and robust liquid crystalline medium for the measurement of residual dipolar couplings," *J. Am. Chem. Soc.*, vol. 122, pp. 5224-5225, 2000.
- [30] Y. Habibi, A.-L. Goffin, N. Schiltz, E. Duquesne, P. Dubois, *et al.*, "Bionanocomposites based on poly([varepsilon]-caprolactone)-grafted cellulose

- nanocrystals by ring-opening polymerization," *J. Mater. Chem*, vol. 18, pp. 5002-5010, 2008.
- [31] T. Saito, Y. Nishiyama, J.-L. Putaux, M. Vignon and A. Isogai, "Homogeneous suspensions of individualized microfibrils from TEMPO-catalyzed oxidation of native cellulose," *Biomacromolecules*, vol. 7, pp. 1687-1691, 2006.
 - [32] P. Hajji, J. Y. Cavaillé, V. Favier, C. Gauthier and G. Vigier, "Tensile behavior of nanocomposites from latex and cellulose whiskers," *Polym. Compos.*, vol. 17, pp. 612-619, 1996.
 - [33] W. Helbert, J. Y. Cavaillé and A. Dufresne, "Thermoplastic nanocomposites filled with wheat straw cellulose whiskers. Part I: processing and mechanical behavior," *Polym. Compos.*, vol. 17, pp. 604-611, 1996.
 - [34] L. Heux, G. Chauve and C. Bonini, "Nonflocculating and chiral-nematic self-ordering of cellulose microcrystals suspensions in nonpolar solvents," *Langmuir*, vol. 16, pp. 8210-8212, 2000.
 - [35] M. A. S. Azizi Samir, F. Alloin, J.-Y. Sanchez, N. El Kissi and A. Dufresne, "Preparation of cellulose whiskers reinforced nanocomposites from an organic medium suspension," *Macromolecules*, vol. 37, pp. 1386-1393, 2004.
 - [36] N. Lin, G. Chen, J. Huang, A. Dufresne and P. R. Chang, "Effects of polymer-grafted natural nanocrystals on the structure and mechanical properties of Poly(lactic acid): a case of cellulose whisker-graft-polycaprolactone," *J. Appl. Polym. Sci.*, vol. 113, pp. 3417-3425, 2009.
 - [37] G. Morandi, L. Heath and W. Thielemans, "Cellulose nanocrystals grafted with polystyrene chains through surface-initiated atom transfer radical polymerization (SI-ATRP)," *Langmuir*, vol. 25, pp. 8280-8286, 2009.
 - [38] N. L. Garcia de Rodriguez, "Sisal cellulose whiskers reinforced polyvinyl acetate nanocomposites," *Cellulose*, vol. 13, pp. 261-270, 2006.
 - [39] M. A. S. Azizi Samir, "Tangling effect in fibrillated cellulose reinforced nanocomposites " *Macromolecules*, vol. 37, pp. 4313-4316, 2004.

- [40] D. Bordel, J.-L. Putaux and L. Heux, "Orientation of native cellulose in an electric field," *Langmuir*, vol. 22, pp. 4899-4901, 2006.
- [41] M. A. S. Azizi Samir, "Plasticized nanocomposite polymer electrolytes based on poly(oxyethylene) and cellulose whiskers," *Electrochimica Acta*, vol. 49, pp. 4667-4677, 2004.
- [42] M. A. S. Azizi Samir, "High performance nanocomposite polymer electrolytes," *Compos. Interfaces*, vol. 13, pp. 545-559, 2006.
- [43] Y. Habibi, A.-L. Goffin, N. Schiltz, E. Duquesne, P. Dubois, *et al.*, "Bionanocomposites based on poly([varepsilon]-caprolactone)-grafted cellulose nanocrystals by ring-opening polymerization," *J. Mat. Chem.*, vol. 18, pp. 5002-5010, 2008.
- [44] D. Dubief, E. Samain and A. Dufresne, "Polysaccharide microcrystals reinforced amorphous poly(β -hydroxyoctanoate) nanocomposite materials," *Macromolecules*, vol. 32, pp. 5765-5771, 1999.
- [45] K. Oksman, "Manufacturing process of cellulose whiskers/polylactic acid nanocomposites," *Compos. Sci. Technol*, vol. 66, pp. 2776-2784, 2006.
- [46] J. R. Capadona, K. Shanmuganathan, D. J. Tyler, S. J. Rowan and C. Weder, "Stimuli-responsive polymer nanocomposites inspired by the sea cucumber dermis," *Science*, vol. 319, pp. 1370-1374, 2008.
- [47] K. Shanmuganathan, J. R. Capadona, S. J. Rowan and C. Weder, "Bio-inspired mechanically-adaptive nanocomposites derived from cotton cellulose whiskers," *J. Mater. Chem.*, vol. 20, pp. 180-186, 2010.
- [48] G. Siqueira, J. Bras and A. Dufresne, "Cellulose Whiskers versus microfibrils: influence of the nature of the nanoparticle and its surface functionalization on the thermal and mechanical properties of nanocomposites," *Biomacromolecules*, vol. 10, pp. 425-432, 2008.
- [49] A. Bendahou, Y. Habibi, H. Kaddami and A. Dufresne, "Physico-chemical characterization of palm from phoenix dactyliferaL, preparation of cellulose

- whiskers and natural rubber based nanocomposites," *J. Biobased. Mater. Bio*, vol. 3, pp. 81-90, 2009.
- [50] N. Ljungberg, C. Bonini, F. Bortolussi, C. Boisson, L. Heux, *et al.*, "New nanocomposite materials reinforced with cellulose whiskers in atactic polypropylene: effect of surface and dispersion characteristics," *Biomacromolecules*, vol. 6, pp. 2732-2739, 2005.
- [51] A. Bendahou, Y. Habibi, H. Kaddami and A. Dufresne, "Physico-chemical characterization of palm from phoenix dactylifera, preparation of cellulose whiskers and natural rubber based nanocomposites," *J. Biobased. Mater. Bio*, vol. 3, pp. 81-90, 2009.
- [52] J. Ji, G. Sui, Y. Yu, Y. Liu, Y. Lin, *et al.*, "Significant improvement of mechanical properties observed in highly aligned carbon-nanotube-reinforced nanofibers," *J. Phys. Chem. C*, vol. 113, pp. 4779-4785, 2009.
- [53] K. R. Vijaya, "Alignment of carbon nanotubes and reinforcing effects in nylon-6 polymer composite fibers," *Nanotechnology*, vol. 19, p. 245703, 2008.
- [54] X. Q. Chen, "Aligning single-wall carbon nanotubes with an alternating-current electric field," *Appl. Phys Lett*, vol. 78, pp. 3714-16, 2001.
- [55] C. A. Martin, "Electric field-induced aligned multi-wall carbon nanotube networks in epoxy composites," *Polymer*, vol. 46, pp. 877-86, 2005.
- [56] P. Cheol and Park, "Aligned single-wall carbon nanotube polymer composites using an electric field," *J. Polym. Sci., Part B: Polym. Phys.*, vol. 44, pp. 1751-62, 2006.
- [57] S. Banda, "Electric field manipulation of polymer nanocomposites: processing and investigation of their physical characteristics," Texas A&M University Ph.D., Texas A&M University, United States -- Texas, 2008.
- [58] K. Bubke, "Optical anisotropy of dispersed carbon nanotubes induced by an electric field," *Appl. Phys. Lett*, vol. 71, pp. 1906-1908, 1997.

- [59] J. M. Hilding, "Alignment of dispersed multiwalled carbon nanotubes in low strength AC electrical fields," *J. Nanosci. Nanotechnol.*, vol. 5, pp. 742-6, 2005.
- [60] J. Evans, "Alignment of high-aspect ratio colloidal gold nanoplatelets in nematic liquid crystals," *J. Appl. Phys.*, vol. 110, p. 033535-7, 2011.
- [61] A. Sharma, "A new method of chaining carbon nanofibers in epoxy," *Nanotechnology*, vol. 19, p. 325606-4, 2008.
- [62] T. Ebeling, M. Paillet, R. Borsali, O. Diat, A. Dufresne, *et al.*, "Shear-induced orientation phenomena in suspensions of cellulose microcrystals, revealed by small angle x-ray scattering," *Langmuir*, vol. 15, pp. 6123-6126, 1999.
- [63] Y. Habibi, T. Heim and R. Douillard, "AC electric field-assisted assembly and alignment of cellulose nanocrystals," *J. Polym. Sci., Part B: Polym. Phys.*, vol. 46, pp. 1430-1436, 2008.
- [64] L. E. Wise, M. Murphy and A. A. D'Addicco, "Chlorite holocellulose, its fractionation and bearing on summative wood analysis and on studies on hemi-celluloses," *Pap. Trade. J.*, vol. 122, pp. 35-43, 1946.
- [65] R. H. Marchessault, F. F. Morehead and N. M. Walter, "Liquid crystal systems from fibrillar polysaccharides," *Nature*, vol. 184, pp. 632-633, 1959.
- [66] M.-K. Yeh, N.-H. Tai and J.-H. Liu, "Mechanical behavior of phenolic-based composites reinforced with multi-walled carbon nanotubes," *Carbon*, vol. 4, pp. 1-9, 2006.
- [67] J. C. Halpin, "Stiffness and expansion estimates for oriented short fiber composites," *J. Compos. Mater.*, vol. 3, pp. 732-734, 1969.
- [68] M. A. S. Azizi Samir, L. Chazeau, F. Alloin, J. Y. Cavail  , A. Dufresne, *et al.*, "POE-based nanocomposite polymer electrolytes reinforced with cellulose whiskers," *Electrochimica Acta*, vol. 50, pp. 3897-3903, 2005.

- [69] M. Özgür Seydibeyoğlu and K. Oksman, "Novel nanocomposites based on polyurethane and micro fibrillated cellulose," *Compos. Sci. Technol.*, vol. 68, pp. 908-914, 2008.
- [70] T. Saito, "Cellulose nanofibers prepared by TEMPO-mediated oxidation of native cellulose," *Biomacromolecules*, vol. 8, pp. 2485-2491, 2007.
- [71] T. Saito, "Homogeneous Suspensions of Individualized microfibrils from TEMPO-catalyzed oxidation of native cellulose," *Biomacromolecules*, vol. 7, pp. 1687-1691, 2006.
- [72] P. L. Bragd, H. van Bekkum and A. C. Besemer, "TEMPO-mediated oxidation of polysaccharides: survey of methods and applications: catalytic conversion of renewables. Guest editors: Herman van bekkum and pierre gallezot," *Top. Catal.*, vol. 27, pp. 49-66, 2004.

APPENDIX

Although MFCs have been studied for over 10 years, they have attracted a lot of attention recently because researchers have prepared very high aspect ratio MFCs that have been shown to significantly improve mechanical properties.

The following section will include discussion on the use of MFCs as mechanical reinforcements and our preliminary work on the dispersion of MFCs.

Background

Microfibrillated cellulose

Grunert et al. reported cellulose acetate butyrate matrix reinforced with 10 wt% of MFC showed 94 and 2000% increase in storage modulus below and above T_g as shown in Figure 1[21]. The study does not address the reason behind the increase in modulus. The authors said further characterization to find if the increase in modulus is due to good filler-matrix adhesion or percolative network held together by hydrogen bonding are being investigated.

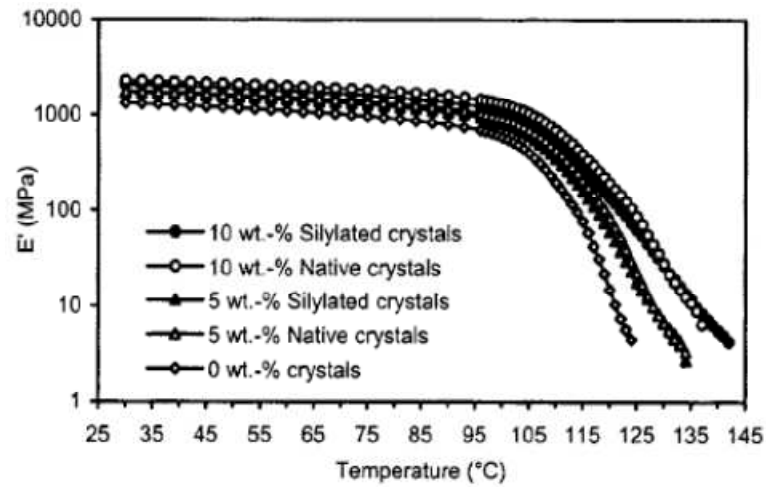


Figure A1: Storage modulus as a function temperature [21].

Seydibeyoglu et al reinforced polyurethane (PU) with hard wood MFCs and studied the mechanical reinforcement [69]. They used a novel process to make fibrillated micro and nano cellulose fibers. They reported a tensile strength increase of 200% for the PU- Cellulose micro fibrils as compared to pure PU. The addition of 8.5 wt% cellulose fi The to the PU matrix increased the Elastic modulus value by 300% and with 18.7 wt% the modulus increased 500%. Table 1 shows mechanical properties of the nanocomposites. The nanofibrils showed to be more effective reinforcement than the micro fibril celluloses. The strength increased from 5 MPa for neat PU to 28 MPa (~ 500%) for the PU-cellulose nanofibril composite, and the modulus increased from 25 to 725 MPa, a 3000% increase.

Table A1: Mechanical Properties of neat PU and prepared composites [69]

Sample	E-modulus (MPa)	Max strength (MPa)
PU	25 ± 0.3	5 ± 0.4
PU-CF1	107 ± 0.8	11 ± 0.2
PU-CF2	144 ± 0.6	15 ± 0.3
PU-CNF1	93 ± 0.7	5 ± 0.2
PU-CNF2	725 ± 1.3	28 ± 0.5

More recently, Sequeira et al compared CWs and MFCs and chemically modified MFCs reinforced polycaprolactone (PLA) composites to study the effect of their reinforcement [48]. The mechanical properties of ensuing composite films were reported to have increased in terms of both stiffness and ductility. Figure 2 shows the elastic modulus, tensile strength and ductility as a function of concentration. The modulus and tensile strength of the modified MFC reinforced composites were reported to be the highest as compared to the CWs reinforced composites followed by MFCs composites.

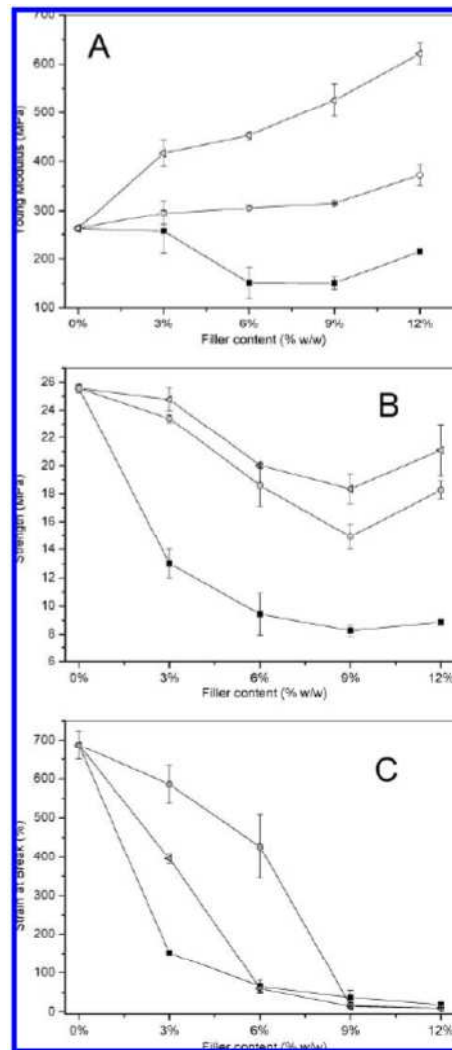


Figure A2: Evolution of the Young's modulus (A), strength (B), and strain at break (C) for PCL-based nanocomposites vs. filler (whisker or MFC) [48].

However, the ductility of the CWs reinforced composites was found to be higher than modified MFC followed by MFC reinforced PLA composites. To summarize, MFC reinforced composites showed improvement in mechanical properties. The driving for the significant improvement was attributed to the formation of 3D structure beyond the

percolation threshold. Similar to CWs significant improvements in mechanical properties were typically achieved with high concentrations of CWs (10% or more).

In recently published articles by Saito et al it was reported that 2,2,6,6-tetramethylpiperidine-1-oxyl (TEMPO)-mediated oxidation of cellulose fibers, allowed for mechanical disintegration of the oxidized fibers in aqueous suspensions [70-71]. TEMPO is a highly stable nitroxyl radical which is used extensively in the selective oxidation of primary alcohols to corresponding aldehydes and carboxylic acids. In aqueous environments, TEMPO catalyzes the conversion of carbohydrate primary alcohols to carboxylate ($\text{COO}^- \text{Na}^+$) functionalities in the presence of a primary oxidizing agent e.g. sodium hypochlorite (NaOCl) [72]. In the studies by Saito et al. three to four nanometer-wide and several hundred nanometers to a few microns-long nanofibrils were obtained without any loss to the nanocellulose degree of crystallinity [70-71].

Results

Dispersion

Transmission electron microscopy

TEM was done to see the effect of oxidation time on the characteristics of native cellulose in terms of dimensions. TEM images were obtained for native cellulose oxidized for 5, 60 and 120 minutes. Figure 3 shows the TEM of native cellulose at 5 minutes of oxidation time. As expected, significant bundling and agglomeration was observed because only a small percentage of primary alcohols undergo the reaction. The bundling and agglomeration shown is similar to MFCs obtained from just mechanical treatment. As the oxidation time is increased to 60 minutes, exfoliated fibril structures were observed. This is because after 60 minutes more primary alcohols have converted to carboxylate ($\text{COO}^- \text{Na}^+$) functionalities and the repulsion between the COO^- functionalities leads to exfoliation as shown in Figure 4. However, the diameter of the fibrils structure is around 100 nm showing that there are still bundles present.

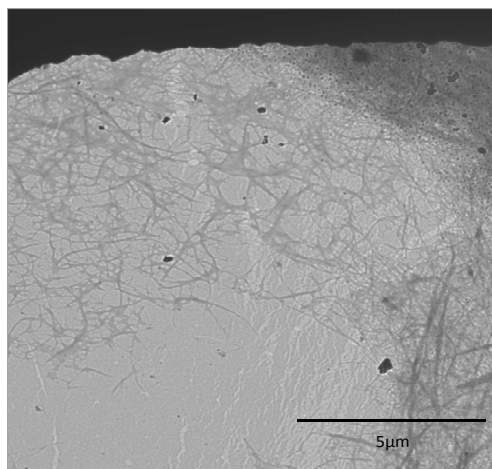


Figure A3: TEM of native cellulose oxidized for 5 minutes.

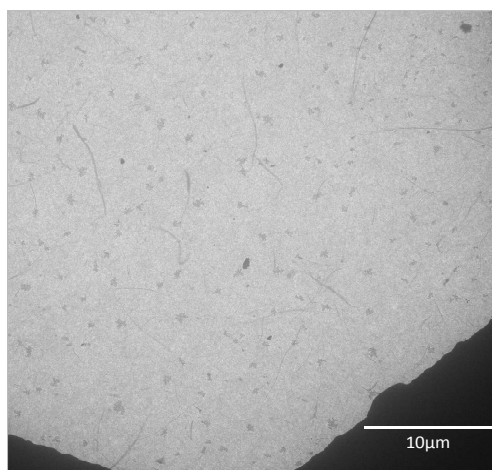


Figure A4: TEM of native cellulose oxidized for 60 minutes.

As the oxidation time is increased to 2 hours further exfoliation was observed with length ranging from 2-4 microns and diameters ranging from 30-40nm as shown in Figure 5. We expect to individually disperse the MFCs with high power sonication.

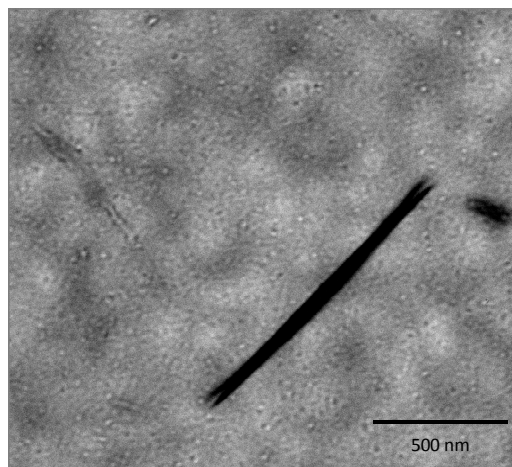


Figure A5: TEM of native cellulose oxidized for 120 minutes.

FTIR measurements were performed to see the level of oxidation achieved on the MFCs and APS modified. Figure 6 shows the FTIR plot for pristine and oxidized MFCs. The black, blue, red and green lines show the FTIR spectra's of pristine MFCs, 5 minutes, 1 hour and 2 hours of oxidation respectively. In these spectra, the arrowed band near 1730cm^{-1} corresponds to the C=O stretching frequency of carboxyl groups in their acidic form. Please note the absence of the 1730 cm^{-1} in the case of the pristine MFCs, which is to be expected. As the MFCs are oxidized for the different cases a peak at 1730cm^{-1} is observed and this peak increases in intensity as the oxidation time is increased.

Figure 7 shows the FTIR plot for pristine and oxidized MFCs. The black and green lines show the FTIR spectra's of pristine CWs and 10 hours of oxidation. As in the case of the MFCs, a band near 1730cm^{-1} corresponding to the C=O stretching frequency of carboxyl groups in their acidic form was observed for the oxidized CWs.

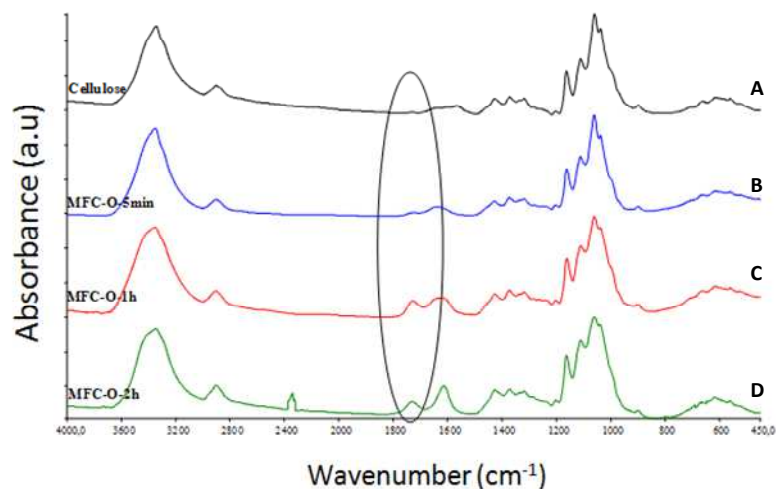


Figure A6: FT-IR spectrum of MFCs: (A) Non-oxidized and oxidized at different times: (B) 5min, (C) 1 Hour, (D) 2 Hours.

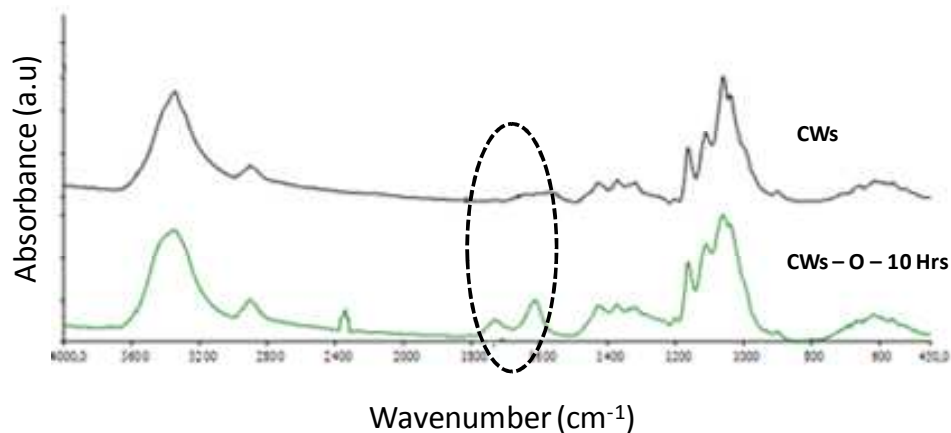


Figure A7: FT-IR spectrum of pristine CWs and oxidized CWs.

UV-Vis spectroscopy was performed on the MFCs to get information on the size and transparency of the various oxidized MFCs. After every three cycles, a small sample of the MFCs was taken to compare the transmittance as a function of number of cycles.

Figure 8 shows the plot of transmittance vs wavenumber for the 5 minutes oxidation case. It was noted that a strong gel is achieved when defibrillation occurs leading to nanofibrillation. It can be seen from Figure 8 that the number of passes notably affects the amount of the nonfibrillated material. We observed an increase in transmittance as a function of number of cycles. The transmittance increases for approximately 14% at 0 cycles to 50 % at low and 90% at high wavenumbers. This behavior was observed for the 1 and 2 hours oxidation cases to as shown in Figure 9 and 10. Significant improvement in transmittance was observed for at 1 and 2 hours as compared to the 5 minutes case. For the 1 hour case, the transmittance improves from 10% for 0 cycles to 78% at low and 100% at high wavenumbers.

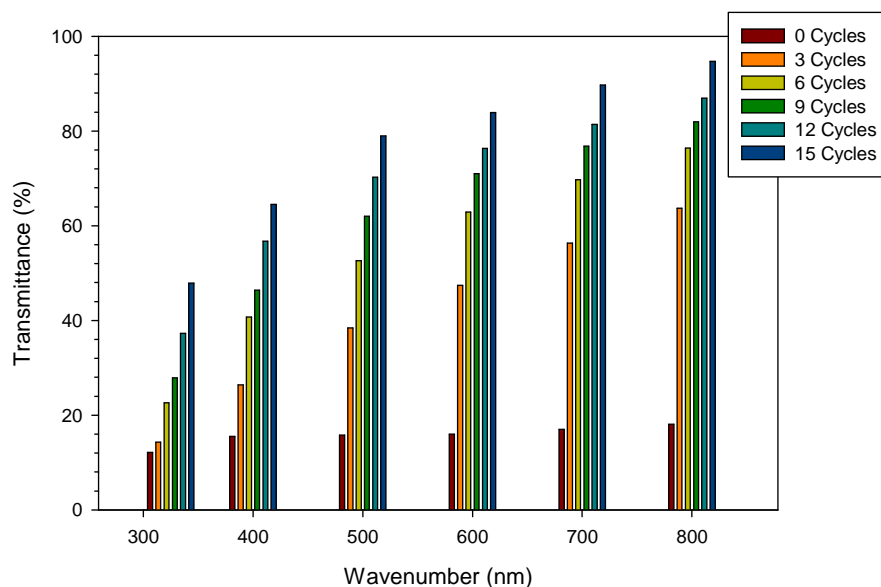


Figure A8: UV-Vis spectroscopy after 5 minutes oxidation as a function of number of cycles.

For all samples a transparency gel is obtained after 3 passes, the fairly higher transparency degree is observed for the highest oxidation degree (2hours), namely for the sample with carboxylic content 774 $\mu\text{mol/g}$.

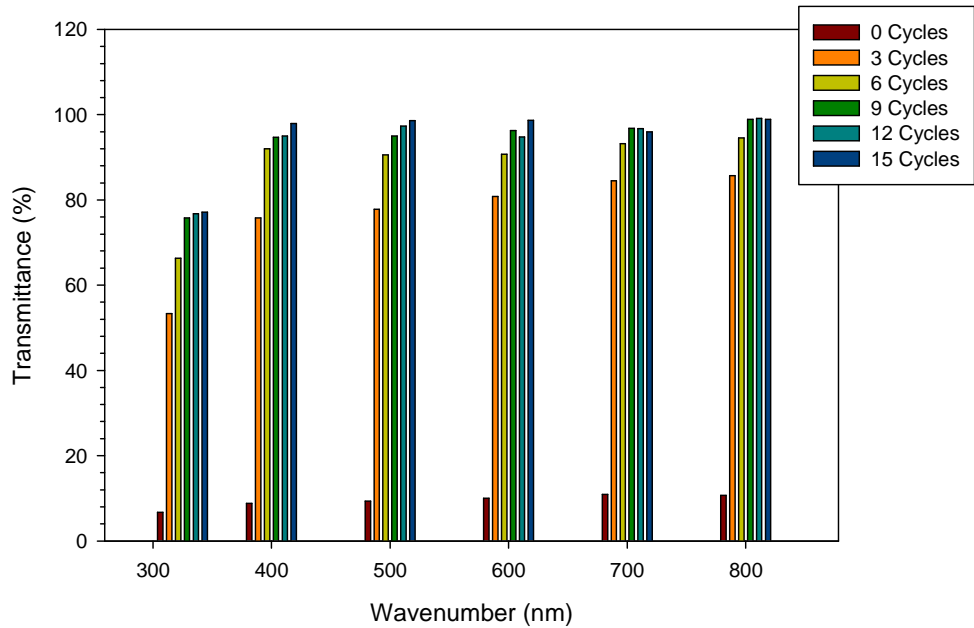


Figure A9: UV-Vis spectroscopy after 1 hour oxidation as a function of number of cycles.

Further evidence of the effect of the homogenization condition on the transparency of the nanofibrillated suspension is depicted from UV-Vis transmittance spectra of diluted suspension (Figure 10). As previously observed for the samples homogenized at 700 bar and after 3 cycles, the highest transmittance is noted for the highest level of carboxylic content. For the 2 hours case, the transmittance improves from 10% for 0 cycles to 84% at low and 100% at high wavenumbers. This significant

increase in transmittance is primarily due to the good nanofibrillation and dispersion of the MFCs.

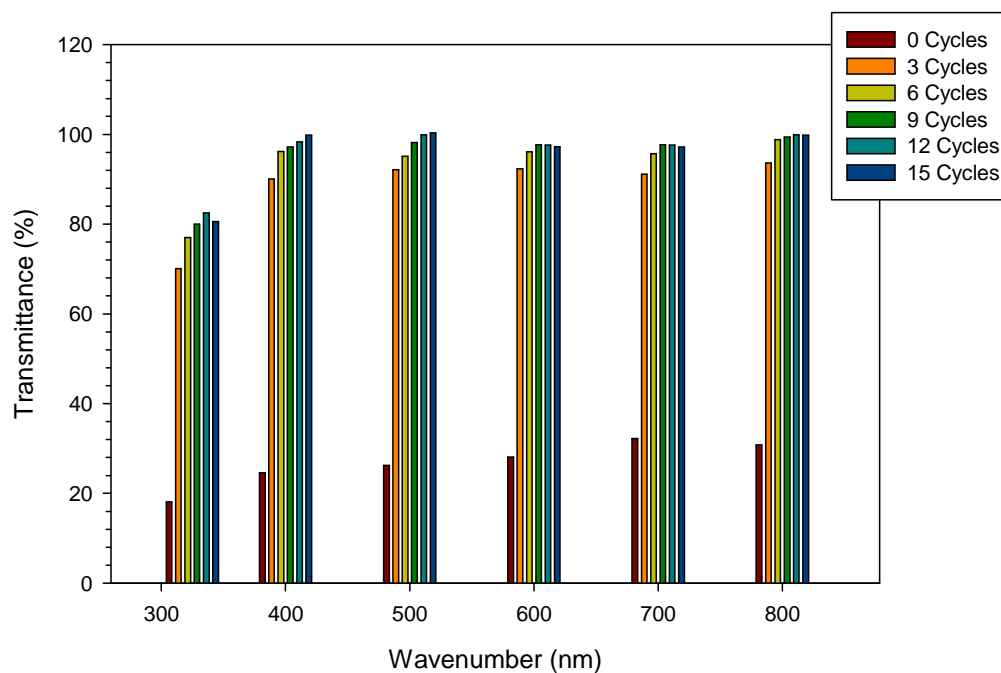


Figure A10: UV-Vis spectroscopy for 2 hours oxidation as a function of number of cycles.

VITA

Name: Sanjay Varma Kalidindi

Address: H. R. Bright Building, Rm701, Ross Street – TAMU 3141, College Station, TX, 77843-3141

Email Address: svkalidindi@mail.com

Education: B.E, Mechanical Engineering, Vellore Engineering College, 2004.
M.S, Mechanical Engineering, University of Texas-Pan American, 2006
Ph.D, Material Science and Engineering, Texas A&M University, 2012.

Journal Publications:

1. **S. Kalidindi**, Z. Ounaies, H. Kaddami, 2011, “Nanocomposites with Oriented Fillers: Electric Field-Manipulation of Cellulose Whiskers in Polyvinyl Acetate”, (Manuscripts in Preparation for Biomacromolecules)
2. **S. Kalidindi**, J. Dowden, Z. Ounaies, 2011, “Single Walled Carbon Nanotube Reinforced High Density Polyethylene Composites by Solution Casting”, (Submitted to Macromolecular Materials and Engineering).
3. **S. Kalidindi**, Z. Ounaies, Kaddami. H, 2010, “Toward the Preparation of Nanocomposites with Oriented Fillers: Electric Field-Manipulation of Cellulose Whiskers in Silicone Oil”, Smart Mater. Struct. 19 (2010) 094002.